



1

2

3

4

5

6

7

8

9

10

11

12 An assessment of natural methane fluxes simulated by the
13 CLASS-CTEM model

14

15 Vivek K. Arora¹, Joe R. Melton², and David Plummer¹.

16

17 ¹Canadian Centre for Climate Modelling and Analysis, Environment and Climate Change Canada,
18 University of Victoria, Victoria, B.C., V8W 2Y2, Canada

19

20

21 ²Climate Research Division, Environment and Climate Change Canada,
22 Victoria, B.C., Canada

23

24

25

26



27

28 **Abstract**

29

30 Natural methane emissions from wetlands and fire, and soil uptake of methane, simulated
31 using the Canadian Land Surface Scheme and Canadian Terrestrial Ecosystem (CLASS-
32 CTEM) modelling framework, over the historical 1850-2008 period, are assessed by using a
33 one box model of atmospheric methane burden. This one box model also requires
34 anthropogenic emissions and the methane sink in the atmosphere to simulate the historical
35 evolution of global methane burden. For this purpose, global anthropogenic methane
36 emissions for the period 1850-2008 were reconstructed based on the harmonized
37 representative concentration pathway (RCP) and Emission Database for Global Atmospheric
38 Research (EDGAR) data sets. The methane sink in the atmosphere is represented using bias-
39 corrected methane lifetimes from the Canadian Middle Atmosphere Model (CMAM). The
40 resulting evolution of atmospheric methane concentration over the historical period compares
41 reasonably well with observation-based estimates. The modelled natural emissions are also
42 assessed using an inverse procedure where the methane lifetimes required to reproduce the
43 observed year-to-year increase in observed atmospheric methane burden are calculated based
44 upon the global anthropogenic and modelled natural emissions that we have used here. These
45 calculated methane lifetimes over the historical period fall within the uncertainty range of
46 observation-based estimates. The present-day (2000-2008) values of modelled methane
47 emissions from wetlands and fire, methane uptake by soil, and the budget terms associated
48 with overall anthropogenic and natural emissions are consistent with estimates reported in a
49 recent global methane budget that is based on top-down approaches constrained by observed
50 atmospheric methane burden. The modelled wetland emissions increase over the historical
51 period in response to both increase in precipitation and increase in atmospheric CO₂
52 concentration. This increase in wetland emissions over the historical period yields evolution
53 of the atmospheric methane concentration that compares better with observation-based values
54 than the case when wetland emissions are held constant over the historical period.

55

56

57



58	Contents	
59		
60	1. Introduction.....	4
61	2. Model, data and experimental set up	7
62	2.1 The CLASS-CTEM model and its forcing and evaluation data sets.....	7
63	2.1.1 The CLASS-CTEM model	7
64	2.1.2 Forcing data for the CLASS-CTEM model.....	15
65	2.1.3 Observation and model-based data for CLASS-CTEM evaluation.....	16
66	2.2 Atmospheric methane – one box model, anthropogenic emissions and lifetime	19
67	2.2.1 One-box model of atmospheric methane.....	19
68	2.2.2 Anthropogenic methane emissions.....	21
69	2.2.3 Lifetime of atmospheric methane	23
70	2.3 The experimental setup	27
71	2.3.1 Equilibrium pre-industrial simulation	27
72	2.3.2 Transient historical simulation	27
73	3. Results.....	28
74	3.1 Time evolution of simulated global natural methane fluxes	28
75	3.2 Evaluation of simulated global natural methane fluxes	30
76	3.3 Geographical distribution of wetland extent	33
77	3.4 Geographical distribution of simulated natural fluxes	34
78	3.5 Regional evaluation over West Siberia lowlands.....	35
79	3.6 Evaluation of present-day global methane budget	38
80	4. Discussion and conclusions	39
81		
82		



83 **1. Introduction**

84

85 Earth system models (ESMs) represent physical climate system processes and their
86 interactions with biogeochemical processes focusing primarily on the carbon cycle in the
87 context of carbon dioxide (CO₂). These models are able to project how the atmospheric
88 concentration of carbon dioxide ([CO₂]) will change in response to changes in anthropogenic
89 CO₂ emissions or alternatively diagnose anthropogenic CO₂ emissions required to achieve a
90 specific CO₂ concentration pathway (Jones et al., 2013). This capability is achieved by
91 modelling [CO₂] as a prognostic variable which itself requires modelling of the surface-
92 atmosphere exchange of CO₂ and hence the need for land and oceanic carbon cycle
93 components in ESMs (Arora et al. 2013; Friedlingstein et al. 2006; Friedlingstein et al. 2014).
94 While most ESMs include the capability of modelling [CO₂] as a prognostic variable there
95 are only a handful of ESMs which are beginning to treat the atmospheric concentration of
96 methane, ([CH₄]), as a fully prognostic variable (Collins et al., 2011; Shindell et al., 2013).

97

98 The [CH₄] has increased from 722 ± 25 ppb in 1750 to 1803 ± 2 ppb in 2011. The [CO₂] has
99 increased globally from 278 (276–280) ppm in 1750 to 390.5 (390.3–390.7) ppm in 2011.
100 The greater global warming potential of CH₄ compared to CO₂, has made methane the second
101 most radiatively important greenhouse gas (GHG) after carbon dioxide CO₂. The CO₂
102 radiative forcing for the period 1750-2011 is 1.82 W/m² (associated with ~112 ppm increase),
103 while the radiative forcing for CH₄ over the same period is 0.48 W/m² (associated with ~1081
104 ppb = 1.08 ppm increase) (Myhre et al., 2013). Since methane is a short-lived GHG with an
105 atmospheric lifetime of around 9 years (compared to CO₂ which has an atmospheric lifetime
106 of around 100-200 years), mitigation of anthropogenic CH₄ emissions can lead to a decrease
107 in its atmospheric concentration within a timeframe of 10-20 years. As a result methane is



108 considered a short-lived climate forcer (SLCF) and therefore reduction in its anthropogenic
109 emissions offers an attractive and potentially viable target for short-term climate change
110 mitigation policies (Shindell et al., 2012). To be able to address climate benefits of reduction
111 in anthropogenic CH₄ emissions within the framework of comprehensive ESMs, however, it
112 is necessary to model [CH₄] as a prognostic variable in these models.

113

114 Treatment of [CH₄] as a fully prognostic variable in ESMs is hindered by at least two factors.
115 First, the global CH₄ budget is not as well understood as for CO₂. Our lack of ability to close
116 the present-day global CH₄ budget is illustrated in Saunois et al. (2016) who present a recent
117 synthesis of several studies and summarize the present-day global CH₄ budget. Saunois et al.
118 (2016) show a large discrepancy between total CH₄ emissions, from both anthropogenic and
119 natural sources, for the 2003-2012 period as inferred from the top-down atmospheric
120 inversion-based approaches (558 Tg CH₄/yr) and those based on bottom-up modelling and
121 other approaches (736 Tg CH₄/yr). The primary reason for this discrepancy is that there are
122 multiple sources of both natural and anthropogenic CH₄ emissions so the bottom-up
123 approaches that add up all the individual sources inevitably give larger total emissions than
124 top-down approaches that are constrained by the atmospheric CH₄ burden and its loss in the
125 atmosphere. Second, unlike CO₂, CH₄ has a sink in the atmosphere which requires
126 representation of atmospheric chemistry in ESMs to properly account for the removal of CH₄
127 and feedbacks of methane on chemistry. CH₄ is destroyed in the troposphere and stratosphere
128 due to its reaction with OH radicals and chlorine. This is typically very computationally
129 expensive to represent. As an example, the model years per wall clock day simulated by
130 second generation Canadian Earth System Model (CanESM2; Arora et al., 2011) are reduced
131 by a factor of around six when atmospheric chemistry is turned on.

132



133 Despite these two challenges there are ways forward to model [CH₄] as a fully prognostic
134 variable and be able to use comprehensive ESMs to ask questions that the climate modelling
135 community has asked so far in the context of CO₂. For example, how would future [CH₄]
136 change in response to changes in anthropogenic and natural CH₄ emissions, or alternatively
137 what should anthropogenic CH₄ emissions be to achieve a given CH₄ concentration pathway,
138 all while as anthropogenic CO₂ emissions continue to increase? In terms of emissions, since
139 the top-down estimates of CH₄ emissions from natural and anthropogenic sources are better
140 constrained than the bottom-up estimates they are likely to provide more robust estimates for
141 evaluating ESMs and their CH₄ related components. The expensive atmospheric chemistry
142 modules can be replaced with simple first-order representations of chemical losses or,
143 ignoring the spatial variations in CH₄ concentration, the global average concentration of
144 methane can be simulated with a box model using specified methane life times which are
145 calculated a priori using full 3D chemistry-climate models. Although, of course, using
146 specified CH₄ losses implies that feedbacks of methane on methane loss rates and interactions
147 between atmospheric chemistry and climate can be neglected.

148

149 The CLASS-CTEM modelling framework serves as the land surface component in the family
150 of Canadian ESMs (CanESMs) (Arora et al., 2009, 2011; Arora and Scinocca, 2016)
151 developed by the Department of Environment and Climate Change, Government of Canada,
152 and models the land-atmosphere fluxes of water, energy and CO₂. It consists of the Canadian
153 Land Surface Scheme (CLASS) and the Canadian Terrestrial Ecosystem Model (CTEM). In
154 preparation for modelling [CH₄] as a prognostic variable in future versions of CanESMs we
155 have included several CH₄ related processes in the CLASS-CTEM modelling framework.
156 These include representations of dynamic natural wetlands and their CH₄ emissions, CH₄
157 emissions from fires, and uptake of CH₄ by soils. This paper evaluates the simulated spatial



158 distribution of wetlands as well as the magnitude of CH₄ emissions from wetlands and fires,
159 and CH₄ uptake by soils against their respective present-day observation-based estimates. We
160 also evaluate the simulated time evolution of the global sums of these fluxes for the 1850-
161 2008 period by using a one-box model of atmospheric CH₄ burden. This one-box model
162 requires anthropogenic CH₄ emissions, emissions from other natural sources that aren't
163 modelled in the CLASS-CTEM framework, and a representation of atmospheric sinks. The
164 anthropogenic CH₄ emissions for the period 1850-2008 are obtained by harmonizing the RCP
165 and EDGAR data sets, and natural emissions from sources that aren't modelled are specified.
166 Finally, the atmospheric sink of CH₄ is based on bias-corrected global atmospheric lifetime of
167 CH₄ as computed by the Canadian Middle Atmosphere Model (CMAM). The one-box model
168 of atmospheric CH₄ burden is used to evaluate CLASS-CTEM simulated natural CH₄ fluxes
169 by comparing simulated evolution of global [CH₄] with their observation-based estimates as
170 well as by comparing the CH₄ lifetime required to reproduce the observed evolution of global
171 [CH₄] over the historical period with their observation-based estimates.

172

173 The rest of this paper is organized as follows. A brief description of the CLASS-CTEM
174 modelling framework is presented in Section 2 along with the details of methane related
175 processes that are implemented, the data sets used and the experimental protocol. Results are
176 presented in Section 3 and finally discussion and conclusions are presented in Section 4.

177 **2. Model, data and experimental set up**

178 **2.1 The CLASS-CTEM model and its forcing and evaluation data sets**

179 **2.1.1 The CLASS-CTEM model**

180

181 The CLASS-CTEM modelling framework consists of the Canadian Land Surface Scheme
182 (CLASS) and the Canadian Terrestrial Ecosystem Model (CTEM) which are coupled to each



183 other and which together simulate fluxes of energy, water, CO₂ and now CH₄ at the land-
184 atmosphere boundary. Together, CLASS and CTEM form the land surface component in
185 Canadian Earth System Models - CanESM1 (Arora et al., 2009), CanESM2 (Arora et al.,
186 2011), and CanESM4.2 (Arora and Scinocca, 2016).

187

188 CLASS simulates atmosphere-land fluxes of energy and water and it prognostically
189 calculates the liquid and frozen soil moisture contents, and soil temperature for its soil layers,
190 the liquid and frozen moisture contents and temperature of the single vegetation canopy layer
191 (if present) and the snow water equivalent and temperature of a single snow layer (if present).
192 CLASS is described in detail in Verseghy (1991), Verseghy et al. (1993) and Verseghy
193 (2000). In the version 3.6 of CLASS used here, the thicknesses of the three permeable soil
194 layers are specified as 0.1, 0.25 and 3.75 m, although the model can be configured to use any
195 number of layers with specified thicknesses. The thicknesses of the permeable layers also
196 depend on the depth to the bedrock which is specified on the basis of the global data set of
197 (Zobler, 1986). For example, if the depth to bedrock is only 2 m, then the thicknesses of the
198 permeable soil layers are taken to be 0.1, 0.25 and 1.65 m. The energy and water balance
199 calculations are performed for four plant functional types (PFTs) (needleleaf trees, broadleaf
200 trees, crops and grasses). CLASS operates at a sub-daily time step and a time step of 30
201 minutes is used here.

202

203 CTEM simulates the fluxes of CO₂ at the land-atmosphere boundary and in doing so models
204 vegetation as a dynamic component of the climate system. It models photosynthesis,
205 autotrophic respiratory fluxes from its three living vegetation components (leaves, stem and
206 roots, denoted respectively by L, S and R) and heterotrophic respiratory fluxes from its two
207 dead carbon components (litter and soil carbon, denoted respectively by D and H). The flow



208 of carbon through these five carbon pools is explicitly tracked which allows to calculate the
209 amount of carbon in these pools as prognostic variables. Disturbance through fire and land
210 use change are also modelled. CTEM cannot operate without coupling to CLASS. Its
211 photosynthesis module operates at the same time step as CLASS and requires estimates of net
212 radiation and soil moisture from CLASS. In return, CTEM provides CLASS with
213 dynamically simulated structural attributes of vegetation which are functions of the driving
214 meteorological data. The amount of carbon in the leaves, stem and root components is used to
215 estimate structural attributes of vegetation. The leaf area index (LAI) is calculated from leaf
216 biomass using PFT-dependent specific leaf area (SLA, $\text{m}^2/\text{Kg C}$) which determines the area
217 of leaves that can be constructed per unit leaf carbon biomass (Arora and Boer, 2005a);
218 vegetation height is calculated based on stem biomass for tree PFTs and LAI for grass PFTs
219 (Arora and Boer, 2005a); and rooting depth is calculated based on root biomass (Arora and
220 Boer, 2003). Other than photosynthesis, all terrestrial ecosystem processes in CTEM are
221 modelled at a daily time step. CTEM models its terrestrial ecosystem processes for nine PFTs
222 that map directly to the PFTs used by CLASS. Needleleaf trees in CTEM are divided into
223 deciduous and evergreen for which terrestrial ecosystem processes are modelled separately,
224 broadleaf trees are divided into cold and drought deciduous and evergreen types, and crops
225 and grasses are divided into C_3 and C_4 versions based on their photosynthetic pathways. The
226 version 2.0 of the model is explained in detail in Melton and Arora (2016), while version 2.1
227 is used here which amongst other minor changes includes all methane related processes
228 discussed below.

229

230 The methane related processes implemented in CLASS-CTEM build on the model's existing
231 capabilities. Processes are implemented to be able to dynamically model the geographical



232 distribution of wetlands and their methane emissions, methane emissions from fire and
233 methane uptake by upland soils.

234 **2.1.1.1 Wetland extent**

235

236 The distribution of wetlands is based on a simple formulation which takes into account the
237 topography in a grid cell and its simulated grid-averaged soil moisture content similar to
238 Kaplan (2002). The ETOPO1 digital elevation data (Amante and Eakins, 2009) are used to
239 calculate slopes at 1 arc minute (1/60th degree) resolution. Each 1 arc minute grid cell is
240 assigned a slope that is the average of eight slopes based on its elevation and the elevation of
241 its eight surrounding grid cells. The objective is to find what fraction of a grid cell, at some
242 given resolution, has slopes flatter than a given slope threshold. Figure 1 displays the fraction
243 of each 0.5 degree grid cell with slopes less than the threshold of 0.002 (i.e. 0.2% slope)
244 calculated using 1 arc minute slopes, hereafter referred to as the “flat” fraction of a grid cell
245 (f_s). The flat fraction of grid cell is also shown at the current operational 2.81° resolution of
246 CanESM4.2, which is the spatial resolution we have used in this study. Figure 1 shows that
247 the approach is able to identify the flat regions of the world including the West Siberian and
248 Hudson Bay lowlands, parts of northern Africa and in South America the Pantanal and the
249 region bordering Argentina, Paraguay and Uruguay.

250

251 The flat fraction is the maximum fraction of a grid cell that can potentially become a wetland,
252 if soils are sufficiently wet, and thus a source of CH₄ emissions. As the grid-averaged
253 simulated soil wetness (w) of the top soil layer increases, above a given lower threshold (w_{low})
254 in a grid cell, its wetland fraction (f_w) is assumed to increase linearly until some specified
255 higher soil wetness threshold (w_{high}) up to a maximum value equal to the flat fraction (f_s) in a
256 grid cell.



257
$$f_w = \max\left(0, \min\left(f_s, \left(\frac{w-w_{low}}{w_{high}-w_{low}}\right) f_s\right)\right)$$
 (1)

258

259 Soil wetness ($w = \frac{\theta_l}{\theta_p}$) itself is defined as the ratio of volumetric liquid soil moisture content
260 (θ_l) to the soil porosity (θ_p) for the top soil layer. The remaining fraction of the grid cell
261 ($1 - f_w$) is considered as the upland fraction. As simulated liquid soil moisture in the top soil
262 layer responds to changes in environmental conditions the dynamic wetlands expand and
263 contract. The upper and lower soil wetness thresholds are summarized in Table 1 and adapted
264 to yield realistic geographical and latitudinal distribution of wetland extent compared to
265 observation-based estimates.

266 **2.1.1.2 Wetland methane emissions**

267

268 The dominant controls on methane emissions in nature are considered to be 1) the position of
269 the water table below which methane is produced due to anoxic decomposition of available
270 organic matter and above which methane is oxidized, 2) the soil temperature which
271 determines the rate of decomposition of organic matter, 3) the availability of organic matter
272 itself, and 4) the pathway through which methane is transferred to the atmosphere (through
273 soil via molecular diffusion, through stems of the vascular plants and through ebullition if the
274 water table is above the soil surface). These factors are not completely independent and their
275 relative importance changes as environmental conditions change (Walter and Heimann,
276 2000). The explicit consideration of these factors becomes more important as the spatial
277 scale at which CH₄ emissions are being modelled reduces. For example, Zhu et al. (2014b)
278 show that as the modelling spatial scale reduces from 100 to 5 km, the dominant control on
279 simulated wetland CH₄ emissions switches from soil temperature to water table depth.

280



281 At the current operational resolution of around 2.81° of CanESM (equal to about 310 km at
 282 the equator) we expect dominant controls on methane emissions to be soil moisture, soil
 283 temperature and the availability of organic matter and this allows us to use the simple
 284 approach that we have used here. CH_4 emissions are simulated to occur over the wetland
 285 fraction of the grid cell. The simulated CH_4 emissions from wetlands are calculated by
 286 scaling the heterotrophic respiratory flux (R_h) from model's litter (D) and soil (H) carbon
 287 pools which itself depends on soil temperature, soil moisture, and the available organic
 288 matter. Heterotrophic respiration from the litter and soil carbon pools takes the following
 289 basic form, with the formulation explained in detail in Melton and Arora (2016)

290

$$R_{h,i} = 2.64 \times 10^{-6} \zeta_i C_i f_i(Q_{10}) f_i(\Psi), i = D, H$$

291

$$R_h = R_{h,D} + R_{h,H} \quad (2)$$

292

293 where ζ_i represents the base respiration rate ($\text{kg C (kg C)}^{-1} \text{ year}^{-1}$) at 15°C , C_i is the amount
 294 of carbon in model's litter or soil carbon pool (kg C m^{-2}), $f_i(Q_{10}) = Q_{10}^{0.1(T_i-15)}$ is a Q_{10}
 295 function that models the effect of temperature, T_i is the temperature of litter or soil carbon
 296 pool ($^\circ\text{C}$) and $f_i(\Psi)$ is the function that reduces heterotrophic respiration when soils are too
 297 dry and too wet using the soil matric potential (Ψ) (Melton et al., 2015). The constant 2.64
 298 $\times 10^{-6}$ converts units from $\text{kg C m}^{-2} \text{ yr}^{-1}$ to $\text{mol CO}_2 \text{ m}^{-2} \text{ s}^{-1}$.

299

300 Modelled CH_4 emissions from wetlands, per unit area of a grid cell ($\text{mol CH}_4 \text{ m}^{-2} \text{ s}^{-1}$), are
 301 calculated as

302

$$E_w = R_h f_w \alpha_w \delta_s \quad (3)$$

304



305 where f_w is the wetland fraction in a grid cell mentioned above, α_w is the ratio of wetland to
306 upland heterotrophic respiratory flux, and δ_s converts flux from CO_2 to CH_4 units but also
307 takes into account that some of the CH_4 flux is oxidized in the soil column before reaching
308 the atmosphere. A value of 0.45 is used for α_w since heterotrophic CO_2 respiratory flux over
309 lowlands is typically lower than over uplands due to limitation by increased soil moisture
310 including a high water table level. While the $f_i(\Psi)$ function in equation (1) does reduce
311 heterotrophic respiration when soils are wet it does so using only the grid averaged soil
312 moisture content. Wania et al. (2010) use a preferred value of δ_s equal to 0.1 and Zhu et al.
313 (2014a) found δ_s varies between 0.1 and 0.7 with a mean value of 0.23 when calibrating
314 their model against data from 19 sites. A value of 0.135 is used for δ_s in this study. The
315 product $\alpha_w \delta_s$ thus equals 0.061 which implies that for each $\text{mol CO}_2 \text{ m}^{-2} \text{ s}^{-1}$ of heterotrophic
316 respiratory flux $0.061 \text{ mol CH}_4 \text{ m}^{-2} \text{ s}^{-1}$ is generated over unit area that is deemed wetland. At
317 large spatial scales CH_4 and CO_2 heterotrophic respiratory fluxes are expected to be highly
318 correlated since to the first order they are both governed by temperature and the amount of
319 organic matter available for decomposition (Dalva et al., 2001; Zhu et al., 2014a). In addition,
320 as the spatial scale increases it is possible to ignore the effect of water table depth as Zhu et
321 al. (2014b) illustrate.

322 2.1.1.3 Fire methane emissions

323

324 Fire in CLASS-CTEM is modelled using an intermediate complexity scheme, which
325 represents both natural and human-caused fires, and accounts for all elements of the fire
326 triangle: fuel load, combustibility of fuel, and availability of ignition sources. The fire module
327 accounts for both natural fires caused by lightning and anthropogenic fires which are the
328 result of ignitions caused by humans expressed as a function of population density. Increasing



329 population density increases human-caused fire ignitions but also increases suppression of
330 fire. The suppression of fire represents fire-fighting efforts, landscape fragmentation and
331 other processes which leads to a reduction in area burned and is also modelled as a function
332 of population density. The original fire parametrization is described in Arora and Boer
333 (2005b) which has since been adapted and used in several other DGVMs (Kloster et al.,
334 2010; Li et al., 2012; Migliavacca et al., 2013). The fire module in CTEM v. 2.1 incorporates
335 changes suggested in these studies as well as several new improvements which are
336 summarized in detail in Melton and Arora (2016). The two primary outputs from the fire
337 module are fraction of area burned per grid cell and dry organic biomass burned per unit area
338 (gC m^{-2}). The dry organic matter burned is then multiplied by corresponding emissions
339 factors to obtained emissions (g species m^{-2}) for several species of trace gases and aerosols
340 including methane (CO_2 , CO , CH_4 , H_2 , NH_3 , NO_x , N_2O , total particulate matter,
341 particulate matter less than $2.5 \mu\text{m}$ in diameter, and black and organic carbon). These
342 emissions factors are based on an updated set by Andreae and Merlet (2001) listed in Tables
343 3 and 4 of Li et al. (2012).

344 **2.1.1.4 Soil uptake of methane**

345

346 The methane uptake over soil occurs over the unsaturated (upland) fraction of a grid cell that
347 is not deemed wetland i.e. $(1-f_w)$. The parameterization is based on an exact solution of the
348 one-dimensional diffusion-reaction equation in the near-surface (top) soil layer and described
349 in detail in Curry (2007). Briefly, the methane uptake by soil is a function of diffusion of
350 methane into soil (which depends on atmospheric methane concentration) and its subsequent
351 oxidation by microbes. The diffusion of methane into the soil depends primarily on air filled
352 porosity of the soil and increases as the pore volume filled by liquid and frozen moisture
353 decreases. The oxidation of methane by microbes is a function of both soil moisture and



354 temperature. Oxidation preferably occurs when soils are neither too dry (when microbial
355 activity is limited by low soil moisture) and nor too wet (when microbes are deprived of
356 oxygen). Warmer temperatures favour oxidation of methane in soil and oxidation increases
357 by about 4 times as soil temperature increases from 0 °C to 27.5 °C. Finally, the inhibition of
358 methane uptake in cultivated soils is accounted for by a linear factor that reduces oxidation as
359 crop fraction in a grid cell increases.

360 **2.1.2 Forcing data for the CLASS-CTEM model**

361

362 The CLASS-CTEM model is driven with meteorological data and atmospheric CO₂ and CH₄
363 concentrations. The model also requires geophysical fields for the fractional coverage of nine
364 CTEM PFTs, soil texture and depth to bedrock. The meteorological data are based on version
365 7 of the Climate Research Unit – National Centre for Environmental Prediction (CRU-NCEP)
366 reanalysis dataset (Viovy, 2012). The meteorological variables (surface temperature,
367 pressure, precipitation, wind, specific humidity, and incident short-wave and long-wave
368 radiation fluxes) are available at a spatial resolution of 0.5° × 0.5° and at a six hourly time
369 interval for the period 1901-2015. These data are regridded to a spatial resolution of 2.81°
370 and temporally to a half-hour time step to drive the CLASS-CTEM model. Temperature,
371 pressure, wind, specific humidity, and long-wave radiation are linearly interpolated in time
372 while short-wave radiation is assumed to change with the solar zenith angle with maximum
373 radiation occurring at solar noon. Following Arora (1997) the six-hourly precipitation amount
374 (P , mm/6-hour) is used to estimate the number of wet half-hours in a given six-hour period
375 and the six- hourly precipitation amount is randomly distributed over these wet half hours.
376 Figure 2 shows the annual land-averaged temperature and precipitation (excluding
377 Antarctica) as derived from the CRU-NCEP data. Both temperature and precipitation show



378 an overall increase over the 20th century, that continues into the 21st century, associated with
379 the changing climate.

380

381 The land cover data are used by the model to specify the fractional coverage of CTEM's nine
382 PFTs in each grid cell. These data are based on a geographical reconstruction of the historical
383 land cover driven by the increase in crop area (Arora and Boer, 2010) but using the crop area
384 data based on the LUH2 v1h version of the Hurtt et al (2006) land cover product. The final
385 data set consists of the fractional coverage of CTEM's nine PFTs for the period 1850-2015 at
386 the global scale and at 2.81° spatial resolution. The increase in crop area over the historical
387 period leads to decrease in area of natural vegetation thus leading to deforestation. A fraction
388 of deforested vegetation is burned but deforested biomass is also converted to paper and
389 wood products which decompose over time leading to land use change emissions. These
390 processes are described in detail in Arora and Boer (2010). In context of terrestrial methane
391 budget, an increase in crop area leads to lower methane uptake by soil over the cultivated
392 fraction of a grid cell.

393

394 The globally averaged atmospheric CO₂ and CH₄ concentrations used to drive the model are
395 obtained from the data sets put together for the sixth phase of the Coupled Model
396 Intercomparison Project (CMIP6) and available from input4MIPs web site ([https://esgf-
397 node.llnl.gov/projects/input4mips/](https://esgf-node.llnl.gov/projects/input4mips/)). These data are shown in Figure 3.

398 **2.1.3 Observation and model-based data for CLASS-CTEM evaluation**

399

400 In addition to evaluating the CLASS-CTEM simulated methane emissions from wetlands, fire
401 and methane uptake by soils in the context of the one-box atmospheric CH₄ model as



402 mentioned in section 2.2 below, we also evaluate simulated present-day wetland extent and
403 all modelled methane fluxes directly against other model and observation-based estimates.

404

405 The CLASS-CTEM simulated wetland extent is compared against two data sets: the wetland
406 data from the Global Lakes and Wetlands Database (GLWD; Lehner and Döll, 2004) and a
407 new product that is formed by merging remote sensing based observations of daily surface
408 inundation from the Surface Water Microwave Product Series (SWAMPS; Schroeder et al.,
409 2015) with the static inventory of wetland area from the GLWD. The derivation of the second
410 product is explained in detail in Poulter et al. (2017). SWAMPS provides estimates of
411 fractional surface water based on data from multiple passive and active microwave satellite
412 missions. While open water (e.g. rivers, lakes and ocean) and inundated wetlands comprising
413 of open plant canopies are mapped by satellites, inundation beneath closed forest canopies,
414 and exposed wetlands with water table below the surface cannot be mapped. However,
415 satellite data are able to provide the seasonal cycle which static data sets like GLWD cannot.
416 The merged SWAMPS-GLWD product attempts to overcome limitations of both individual
417 data sets.

418

419 The simulated present-day methane emissions from wetlands and fire, and methane uptake by
420 soil, are compared to top-down estimates compiled by Saunois et al. (2016). We also
421 compare the anthropogenic emissions we have used within the framework of one-box
422 atmospheric methane model (Section 2.2) with estimates from Saunois et al. (2016).

423

424 Finally, we also evaluate the model regionally over the West Siberian Lowlands (WSL). This
425 region is chosen because inversion-based methane fluxes are readily accessible over the
426 region which were compiled and documented for the WETCHIMP-WSL Intercomparison



427 project (Bohn et al., 2015). We compare simulated wetland extent and wetland methane
428 emissions with observation- and inversion-based results from Bousquet et al. (2011), Kim et
429 al. (2011), and Winderlich (2012) and participating models in the Wetland and Wetland CH₄
430 Intercomparison of Models Project (WETCHIMP, Melton et al. (2013)) focused on the West
431 Siberian Lowlands region (WETCHIMP-WSL) (Bohn et al., 2015). Of these the Kim et al.
432 (2011) and Winderlich (2012) are regional inversions. Kim et al. (2011) used wetland
433 methane emissions from Glagolev et al. (2010) at 1° spatial resolution as their prior and used
434 the NIES-TM atmospheric transport model for the period 2002–2007. They derived
435 climatological monthly wetland emissions optimized to match atmospheric methane
436 concentrations obtained by aircraft sampling. Winderlich (2012) used the Kaplan (2002)
437 wetland inventory for prior wetland emissions with the TM3-STILT global inversion system
438 for year 2009. Their posterior monthly wetland emissions were uniquely determined for each
439 grid cell within their domain at 1° spatial resolution and optimized to match atmospheric
440 methane concentrations measured at four tower observation sites located between 58°N and
441 63 °N. The Bousquet et al. (2011) is a global inversion but uses two priors – the first one
442 based on the Matthews and Fung (1987) emissions inventory and the second based on Kaplan
443 (2002). Bousquet et al. (2011) inversion used the Laboratoire de Météorologie Dynamique
444 general circulation model (LMDZ) atmospheric transport model at a 3.75° × 2.5° grid and
445 estimated monthly methane emissions at a 1° spatial resolution for the period 1993–2009.
446 Being a global inversion they optimized atmospheric concentrations relative to global surface
447 observations at several flask stations for methane but also other trace gases. For wetland
448 extent, we compare the CLASS-CTEM simulated wetland extent over the WSL region with
449 models participating in the WETCHIMP-WSL intercomparison, and GLWD and
450 SWAMPS+GLWD products mentioned above but also the Global Inundation Extent from
451 Multi-Satellites (GIEMS; Papa et al., 2010; Prigent et al., 2007) derived from visible and



452 near-infrared and active and passive microwave sensors for the period 1993–2004. In
453 addition, we also use the estimate from Peregon et al., (2009) who used a regional wetland
454 typology map further refined by satellite image classifications to calculate the wetland extent
455 in the WSL region.

456 2.2 Atmospheric methane – one box model, anthropogenic emissions and lifetime

457 2.2.1 One-box model of atmospheric methane

458

459 A one-box model of atmospheric CH₄ is used to evaluate the time evolution of simulated
460 methane emissions from wetlands (E_w), methane emissions from fire (E_f) and the soil uptake
461 of methane (S_{soil}) over the period 1850–2008. The model describes the changes in burden of
462 atmospheric CH₄ (B) as a balance of surface emissions (consisting of natural, E_N , and
463 anthropogenic emissions, E_A) and the atmospheric (S_{atmos}) and surface soil sinks (S_{soil}).

$$464 \quad \frac{dB}{dt} = E_N(t) + E_A(t) - S_{atmos}(t) - S_{soil}(t) \quad (4)$$

465 where t is the time and equation (4) is applied at an annual time step. The atmospheric CH₄
466 burden (B , Tg CH₄) equals 2.78 times [CH₄] (represented in units of parts per billion, ppb)
467 (Denman et al., 2007). The distinction between natural and anthropogenic emissions is not
468 straight-forward for fire which contains emissions due to both natural and human-caused
469 fires. For comparison with Saunio et al. (2016) global CH₄ budget (as shown later in Section
470 3) we consider all emissions from fire as anthropogenic, although the CLASS-CTEM model
471 calculates fire emissions due both to lightning and human-caused ignitions. Natural emissions
472 ($E_N = E_w + E_o$) consist of modelled wetlands emissions (E_w) and emissions from other
473 natural sources (E_o) (including termites, geological sources, wild animals and freshwater)
474 which we specify at 30 Tg CH₄/yr (consistent with but towards the lower end of the range



475 natural emissions, 20-130 Tg CH₄/yr, as deduced by top-down approaches summarized in
 476 Saunois et al. (2016)). The reason for specifying E_o at 30 Tg CH₄/yr is discussed later in
 477 section 4. Anthropogenic emissions ($E_A = E_{A \text{ excl fire}} + E_f$) consist of specified emissions
 478 from all anthropogenic sources excluding fire ($E_{A \text{ excl fire}}$) and fire emissions which we
 479 explicitly model (E_f). Estimation of anthropogenic emissions excluding those from fire and
 480 biomass burning ($E_{A \text{ excl fire}}$) data are explained in section 2.2.2.

481

482 The atmospheric sink S is calculated as a first-order loss process from methane's lifetime
 483 τ_{chem} in the atmosphere as $S_{atmos}(t) = B(t)[1 - \exp(-1/\tau_{chem}(t))]$. An estimate of τ_{chem}
 484 is obtained from the Canadian Middle Atmosphere Model (CMAM) with chemistry and
 485 compared to an observation-based estimate from Prather et al. (2012) as later shown in
 486 Section 2.2.3. With S_{atmos} represented in terms of τ_{chem} equation (4) can be rewritten as

$$487 \quad \begin{aligned} B(t + \Delta t) &= B(t) - B(t)[1 - \exp(-1/\tau_{chem}(t))] + (E_N(t) + E_A(t) - S_{soil}(t))\Delta t \\ &= B(t)[\exp(-1/\tau_{chem}(t))] + (E_N(t) + E_A(t) - S_{soil}(t))\Delta t \end{aligned} \quad (5)$$

488 where $\Delta t = 1$ year. Equation (5) can be used to evaluate simulated natural methane emissions
 489 E_N in two ways. First, when all the terms on the right hand side of equation (5), including an
 490 initial value of $B(t)$, are known then the time evolution of B can be calculated and compared
 491 to its observation-based estimate. Second, if the time evolution of B is specified based on
 492 observations of methane concentration in the atmosphere then the value of τ_{chem} required to
 493 satisfy equation (5) can be calculated (see equation 6) and compared its observation-based
 494 estimate e.g. from Prather et al. (2012).

$$495 \quad \tau_{chem}(t) = -\frac{1}{\log\left(\frac{B(t+\Delta t) - (E_N(t) + E_A(t) - S_{soil}(t))\Delta t}{B(t)}\right)} \quad (6)$$

496



497 In section 3, we have used both these methodologies to assess CLASS-CTEM simulated
498 methane emissions from wetlands (E_w), methane emissions from fire (E_f) and the soil uptake
499 of methane (S_{soil}). Note that equation (5) does not include any term for oceanic methane
500 emissions. Saunio et al. (2016) report a range of 0–5 Tg CH₄/yr, with a mean value of 2 Tg
501 CH₄/yr for oceanic methane emissions. Given the large uncertainty in other components of
502 the global methane budget, and the small magnitude of oceanic methane emissions, we have
503 ignored this term.

504 **2.2.2 Anthropogenic methane emissions**

505

506 The time evolution of global E_A (used in equation 5) for the 1850-2008 period is based on
507 two data sets. The first data set is the decadal representative concentration pathway (RCP)
508 anthropogenic methane emissions data set (version 2.0.5) available at 0.5° spatial resolution
509 for the period 1850-2000 and provided for the fifth phase of the coupled model
510 Intercomparison project (CMIP5) by the International Institute for Applied Systems Analysis
511 (IIASA) (<http://www.iiasa.ac.at/web-apps/tnt/RcpDb>). The value for the first year of each
512 decade is assumed to correspond to the rest of the decade. So the 1850 value corresponds to
513 the 1850-1859 decade, the 1860 value corresponds to the 1860-69 decade and so on. The
514 second anthropogenic methane emissions data set is part of version 4.2 of the Emission
515 Database for Global Atmospheric Research (EDGAR,
516 <http://edgar.jrc.ec.europa.eu/overview.php?v=42>) available at 0.1° spatial resolution and
517 available for the period 1970-2008. These data sets were selected because the RCP data set
518 provides the anthropogenic methane emissions going back to 1850 and the EDGAR data set
519 provides the anthropogenic methane emissions for more recent years since 1970. The
520 EDGAR data set was also chosen because amongst the recent anthropogenic data sets this is



521 the only data set which provides gridded anthropogenic methane emissions at an annual time
522 scale (see Table 1 of Saunio et al (2016)).

523

524 These two data sets are blended (or harmonized) to obtain a consistent time series of annual
525 global anthropogenic methane emissions for the period 1850-2008. First the RCP and
526 EDGAR data are regridded from their 0.5° and 0.1° spatial resolutions, respectively, to the
527 2.81° resolution at which the model is applied. Next all non-biomass burning emission
528 categories are added separately in both data sets to obtain total anthropogenic emissions for
529 each data set. The emissions categories in both data sets are somewhat different as shown in
530 Table 2. Emissions from fire and biomass burning are excluded because CLASS-CTEM
531 simulates CH₄ emissions from fire explicitly. Since our framework requires only total
532 anthropogenic methane emissions (excluding biomass burning) the different emissions
533 categories in the two data sets do not matter. Equation (7) summarizes this harmonization
534 methodology for a given grid cell.

535

$$536 \quad E_{A,RCP \text{ adjusted}}(t) = E_{A,RCP}(t) + \frac{t-1850}{1970-1850} (E_{A,EDGAR}(1970) - E_{A,RCP}(1970)) \quad (7)$$

537

538 where $E_{A,RCP}$ and $E_{A,EDGAR}$ represent annual anthropogenic methane emissions (excluding
539 biomass burning) in the RCP and EDGAR data sets, respectively, $E_{A,RCP \text{ adjusted}}$ represent the
540 adjusted RCP emissions and t is the time in years from 1850 to 1970. The harmonization
541 algorithm adjusts the annual total anthropogenic methane emissions in the RCP data, for each
542 2.81° grid cell, from 1850 to 1970 such that by the time RCP emissions reach 1970 they are
543 the same as the EDGAR's total emissions excluding biomass burning. As a result of this
544 harmonization, the largest change is made to RCP emissions for year 1970 and the smallest
545 change is made for year 1851. The RCP emissions for year 1850 are not changed. The final



546 harmonized time series for E_A is obtained by concatenating $E_{A,RCP}$ adjusted for the period 1850
547 to 1970 and $E_{A,EDGAR}$ for the period from 1971 to 2008.

548

549 Figure 4a shows the harmonized time series of global anthropogenic methane emissions
550 along with the decadal RCP and annual EDGAR emissions (excluding biomass burning). The
551 RCP and EDGAR emissions are fairly similar for the period 1970-1990 but are different after
552 1990. Figures 4b and 4c illustrate how the harmonization works for two selected grid cells
553 based on equation (7). In Figure 4b anthropogenic methane emissions are shown for a land
554 grid cell where emissions first increase and then decrease. In Figure 4c anthropogenic
555 methane emissions are shown for an ocean grid cell, with six orders of magnitude lower
556 emissions than the land grid cell, where emissions more or less continuously increase. In both
557 case, the harmonization ensures that by 1970 the adjusted RCP emissions are same as the
558 EDGAR emissions. Although for the purpose of using E_A in equation (5) only its global
559 values are required, the methodology described here yields a continuous consistent gridded
560 data set of anthropogenic methane emissions for the period of our analysis with no abrupt
561 jumps.

562

563 2.2.3 Lifetime of atmospheric methane

564

565 To use equation (5), for evaluation of CLASS-CTEM simulated annual values of E_w , E_f and
566 S_{soil} over the historical period, time-evolving annual values of τ_{chem} are required. We obtain
567 values of τ_{chem} simulated by the Canadian Middle Atmosphere Model (CMAM). The
568 CMAM is a fully interactive chemistry-climate model (CCM) that is based on a vertically
569 extended version of the third generation Canadian Atmospheric General Circulation Model
570 with a model lid at 95 km (Scinocca et al., 2008). The model contains a description of the



571 important physical and chemical processes of the stratosphere/mesosphere and has been
572 extensively assessed against observations through participation in two phases of the
573 Chemistry-Climate Model Validation (CCMVal) activity (Eyring et al., 2006; SPARC
574 CCMVal, 2010). Of more importance for methane, the chemistry has been extended
575 throughout the troposphere by including cloud corrections on clear-sky photolysis rates,
576 emissions of ozone precursors CO and NO_x (NO + NO₂) including emissions of NO_x from
577 lightning, hydrolysis on specified tropospheric sulphate aerosols and interactive wet and dry
578 deposition. Note that the chemical mechanism currently used in CMAM has not yet been
579 extended to include the chemistry of non-methane hydrocarbons important in the
580 troposphere; only methane chemistry is considered.

581

582 Results from CMAM with tropospheric chemistry have been submitted to the Atmospheric
583 Chemistry and Climate Model Intercomparison Project (ACCMIP) (Lamarque et al., 2013).
584 The experimental design for ACCMIP involved timeslice simulations at various points in
585 time between 1850 and 2100, with simulations for year 2000 conditions used for assessing
586 the model chemical climate against available present-day observations. The ACCMIP
587 intercomparison found that the CMAM produced estimates of tropospheric chemical
588 quantities that fell well within the range of current generation CCMs. For example, the
589 present-day tropospheric ozone burden from CMAM was 323 Tg, versus a multi-model mean
590 of 337 ± 23 Tg, where the range is given as one standard deviation across the 15 participating
591 models (Young et al., 2013). The present-day methane lifetime to reaction with OH in the
592 troposphere was found to be 9.4 years, again well within the range of ACCMIP models of 9.7
593 ± 1.5 years (Naik et al., 2013). However, like the majority of ACCMIP models, the CMAM
594 predicts a too fast removal of CH₄ by OH as compared with our best-estimate from methyl-
595 chloroform decay of 11.2 ± 1.3 years (Prather et al., 2012). As described further below, the



596 calculated CH₄ lifetime to chemical loss from CMAM is therefore scaled to agree with
597 observationally-based estimates before being used in the one box model.

598

599 Time-dependent values of τ_{chem} are derived from a simulation over the 1850-2014 period
600 that uses specified sea-surface temperatures and sea-ice from one member of the five-member
601 historical ensemble performed by CanESM2 for the CMIP5. Data for 2006-2014 was taken
602 from a continuation of that simulation for the RCP 6.0 scenario. Specified anthropogenic and
603 biomass burning emissions of CO and NO_x were taken from the CMIP5 historical database
604 (Lamarque et al., 2010) up to 2000 and for the RCP 6.0 scenario to 2014. Specified
605 concentrations of long-lived greenhouse gases were from Meinshausen et al. (2011),
606 following RCP 6.0 from 2006-2014. Specified stratospheric aerosol surface area density
607 fields, used to account for the effects of large volcanic eruptions, was based on the 1960-2010
608 database created for the Chemistry Climate Model Initiative (CCMI) extended back to 1850
609 following the approach described in Neely III et al. (2016). Solar variability was included by
610 calculating the wavelength-resolved daily variability relative to the long-term average (June
611 1976 – January 2007) from the recommended CMIP6 database (Matthes et al., 2017).

612

613 The observation-based estimate of τ_{chem} is obtained from Prather et al. (2012) who calculate
614 τ_{CH_4} based on equation (8) as

$$615 \quad \frac{1}{\tau_{CH_4}} = \frac{1}{\tau_{OH}} + \frac{1}{\tau_{strat}} + \frac{1}{\tau_{trop-cl}} + \frac{1}{\tau_{soil}} = \frac{1}{\tau_{chem}} + \frac{1}{\tau_{soil}} \quad (8)$$

616 where τ_{OH} (present day value of 11.2 years), τ_{strat} (120 years), $\tau_{trop-cl}$ (200 years) and τ_{soil}
617 (150 years) are the lifetimes associated with the destruction of CH₄ by tropospheric OH
618 radicals, loss in the stratosphere, reaction with tropospheric chlorine and uptake by soils,
619 respectively, which yields a present day (corresponding to year 2010) value of τ_{CH_4} as



620 9.1±0.9 years. τ_{chem} is the methane life time associated with chemical processes in the
621 atmosphere. For the pre-industrial period (corresponding to year 1750), Prather et al. (2012)
622 estimate τ_{CH_4} as 9.5±1.3 years assuming τ_{OH} to be equal to 11.76 years (based on
623 Atmospheric Chemistry and Climate Model Intercomparison Project (ACCMIP) results
624 (Voulgarakis et al., 2013)) and lifetimes associated with other processes are assumed to stay
625 the same. In our study, the methane soil sink is explicitly simulated in the CLASS-CTEM
626 framework and this corresponds to the term $\frac{1}{\tau_{soil}}$ in equation (8). The remaining terms in
627 equation (8) all correspond to atmospheric processes. Removing the $\frac{1}{\tau_{soil}}$ term in equation (8)
628 gives us an observation-based estimate of τ_{chem} making it consistent with CMAM's methane
629 lifetime corresponding only to atmospheric processes and increases the observation-based
630 estimates of pre-industrial and present-day atmospheric CH₄ lifetimes to 10.15±1.45 years
631 and 9.7±1.0 years, respectively.

632

633 Figure 5 compares the τ_{chem} values from CMAM with its observation-based estimate from
634 Prather et al. (2012) and shows that CMAM based estimates are biased low and outside the
635 uncertainty range of observation-based estimates, as mentioned earlier. When used in the
636 one-box model of atmospheric methane, the lower than observed τ_{chem} values will
637 inevitably lead to a higher than observed atmospheric sink (S_{atmos}) and thus lower than
638 observed atmospheric methane concentration even if all the other flux terms (E_N , E_A , and
639 S_{soil}) in equation (5) are realistic. We therefore adjust the CMAM derived values of τ_{chem}
640 upwards by 15% so that they lie within the uncertainty range of observation-based estimates
641 of the τ_{chem} as derived by Prather et al. (2012). These adjusted values of τ_{chem} are also
642 shown in Figure 5.

643



644 **2.3 The experimental setup**

645

646 **2.3.1 Equilibrium pre-industrial simulation**

647

648 The equilibrium pre-industrial simulation was initialized from zero biomass for all PFTs. The
649 fractional coverages of CTEM's nine PFTs for the pre-industrial simulation are based on the
650 land cover product described in section 2.1.2 for year 1850. The model was then driven with
651 1901-1925 CRU-NCEP climate data cycled repeatedly until the model pools reach
652 equilibrium. The early part of the 20th century does not show any significant trends compared
653 to the later part of the 20th century, as seen in Figure 2a, so using the 1901-1925 data to spin
654 up the model to equilibrium for 1850 conditions is reasonable. Atmospheric CO₂ and CH₄
655 concentration levels were set to 285 ppm and 791 ppb, respectively, corresponding to their
656 pre-industrial 1850 levels. This pre-industrial equilibrium simulation yields initial conditions
657 for all CLASS-CTEM prognostic variables for the transient 1851-2015 simulation.

658

659 **2.3.2 Transient historical simulation**

660

661 The transient historical simulation is performed for the period 1851-2015 and its prognostic
662 variables are initialized from the equilibrium pre-industrial simulation as mentioned above.
663 For the period 1851 to 1900 of this simulation the model is driven with meteorological data
664 from 1901-1925 twice similar to what we do for spinning up the model for the pre-industrial
665 simulation. For the period 1901-2015 the meteorological data corresponding to each year are
666 used. Time varying concentrations of atmospheric CO₂ and CH₄ are specified for the period
667 1851-2015. The annual time-varying fractional coverages of C₃ and C₄ crop PFTs in each
668 grid cell are based on LUH2 v1h version of the Hurtt et al (2006) land cover product.



669

670 In this transient simulation, 1) wetland extent and its methane emissions respond to changes
671 in climate but also increases in atmospheric CO₂ concentration (which increases net primary
672 productivity and thus heterotrophic respiration), 2) methane emissions from fire respond to
673 changes in climate, atmospheric CO₂ concentration, population density and land use change,
674 and 3) methane uptake by soil responds to climate, changes in atmospheric CH₄ concentration
675 and changes in crop fraction.

676

677 **3. Results**

678

679 We first show the results from the transient 1851-2015 simulation and evaluate the time-
680 evolution of CLASS-CTEM simulated global natural methane fluxes over the historical
681 period using the one-box model of atmospheric methane described in section 2.2. This is
682 followed by evaluation of model fluxes for the present day against observation-based
683 estimates and for the WSL region using results from other models.

684

685 **3.1 Time evolution of simulated global natural methane fluxes**

686

687 Figure 6 shows the time evolution of simulated annual maximum wetland extent, methane
688 emissions from wetlands and fire, and soil uptake by methane from the 1851-2015 transient
689 historical simulation. In Figure 6: 1) the simulated wetland methane emissions increase by
690 30% over the historical period from about 130 to 169 Tg CH₄/yr from 1850s to the present
691 day (2000-2008) partly due to increase in wetland extent which increases by 8% from 7.5 to
692 8.1 million km² from 1850s to the present day, 2) the simulated fire methane emissions



693 decrease from their 1850s value by 20% from about 34 to 27 Tg CH₄/yr for the present day
694 and 3) the soil methane uptake more than doubles from its 1850s value of about 14 to 29 Tg
695 CH₄/yr for the present day.

696

697 The increase in wetland methane emissions over the historical period is due to an increase in
698 the wetland area, driven by increase in precipitation seen in Figure 2b, but also higher
699 methane fluxes per unit area. The higher methane fluxes per unit area are caused by increase
700 in atmospheric CO₂ concentration which increases both net primary productivity and
701 heterotrophic respiration over the historical period as shown in Figure 7. Since wetland
702 methane emissions are proportional to heterotrophic respiration (R_h) in equation (3) an
703 increase in R_h also increases methane emissions from wetlands. The decrease in methane
704 emissions from wildfires is driven by a decrease in area burned which itself is driven by an
705 increase in crop area and population density over the historical period. The increase in
706 cropland area decreases area burned by wildfires in the model since croplands are not allowed
707 to burn. In the real world cropland area also fragments the landscape which affects the spread
708 of fire. Direct anthropogenic influences on wildfires are more complex since accidental, as
709 well as intentional, human-caused ignitions enhance wildfires while anthropogenic
710 suppression of wildfires decreases area burned and fire related emissions.

711

712 Figure 8 shows that the overall effect of increase in crop area and population density in the
713 model is that area burned increases slightly up to about 1920, and then starts decreasing
714 thereafter and this area burned pattern compares reasonably with the decadal charcoal index
715 from the Global Charcoal Database version 3 (Marlon et al., 2008) for the full length of the
716 historical simulation. Winds and smoke carry charcoal from fires and deposit it onto aquatic
717 sediments and this forms the basis of sediment charcoal indices. The caveat with the



718 comparison with sediment charcoal records is that they provide only a proxy for fire activity
719 and indicate if fire activity is higher or lower relative to a point in time. Figure 8 also
720 compares area burned with estimates from version 4.1s of the Global Fire Emissions
721 Database (Giglio et al., 2013; Randerson et al., 2012) that are based on the satellite record
722 and available only for the short 1997-2014 period. Model and observation-based average
723 burned area over this 1997-2014 period are 483.4 and 485.5 million hectares year⁻¹ and their
724 trends are -5.57 ± 1.25 and -3.43 ± 1.05 million hectares year⁻², respectively. The negative
725 trends indicate burned area has been decreasing. Finally, the increase in methane uptake by
726 soils is primarily the response to an increase in the atmospheric concentration of methane.
727 Diffusion of methane into the soil is directly proportional to its atmospheric concentration
728 (Curry, 2007) which more than doubles from around 790 ppb in 1850 to around 1830 ppb in
729 2015 (Figure 3b).

730

731 3.2 Evaluation of simulated global natural methane fluxes

732

733 We first evaluate the CLASS-CTEM simulated global natural methane fluxes in a forward
734 simulation where all the right hand side terms of equation (5) are specified at an annual time
735 step and the change in atmospheric methane burden $\frac{dB}{dt}$ is calculated every year. Although
736 the CRU-NCEP meteorological data are available to 2015 allowing us to perform offline
737 CLASS-CTEM simulations up until 2015, the last year for which harmonized RCP-EDGAR
738 emissions are available is 2008. We therefore simulate the time evolution of atmospheric
739 methane concentration for the period 1851-2008. In this forward calculation of atmospheric
740 methane burden the one box model may be initialized using the observed 1850 methane
741 concentration or using the 1850 concentration that is in equilibrium with 1850 sinks and



742 sources. The latter is calculated by assuming $\frac{dB}{dt} = 0$ in equation (5) and finding the value of
743 B for all other terms corresponding to their 1850 values. This yields an equilibrium
744 concentration in 1850 of 708 ppb compared to its observation-based value of 791 ppb. An
745 equilibrium methane concentration in 1850 that is lower than observed implies that the 1850
746 emissions are lower and/or the atmospheric methane sink is higher (associated with lower
747 atmospheric methane lifetime in 1850). Regardless, since the lifetime of methane in the
748 atmosphere is only around 10 years the effect of initial conditions disappears by around 1870.
749 This is shown in Figure 9a which compares the simulated evolution of atmospheric methane
750 burden with its observations. Figure 9a shows that overall the simulated increase in methane
751 concentration over the historical period is reasonable compared to observation-based
752 estimates despite the various specified and modelled sources and sinks that contribute to the
753 time evolution of atmospheric methane burden. The simulated values are somewhat
754 overestimated from 1885 to 1980 and underestimated from 1980 to 2005. The increase in
755 observed methane concentration over the 1850 to 2008 period is 998 ppb, while the one box
756 model yields an increase of 1024 ppb when initialized from observed 1850 methane
757 concentration. The year 2008 concentration is calculated to be 1815 ppb compared to the
758 observation-based value of 1790 ppb.

759

760 An alternative approach to evaluate the modelled natural sinks and sources is to specify the
761 rate of increase of atmospheric methane burden according to its observations and calculate
762 the required atmospheric lifetime of methane (excluding the soil sink), given modelled
763 natural sinks and sources, following equation (6) as discussed in section 2.2. These results are
764 shown in Figure 9b, which compares the methane lifetimes required to achieve the observed
765 increase in methane concentration over the historical period (black line) to within ± 5 ppb
766 (shaded area between grey lines) with observation-based estimate of atmospheric methane



767 lifetime based on Prather et al. (2012) and the adjusted atmospheric methane lifetime from
768 CMAM (both of which were shown earlier in Figure 5). Figure 9b shows that for the most
769 part, the calculated atmospheric methane lifetime stays within the uncertainty of observation-
770 based estimates. More over the temporal trend after 1900 in calculated atmospheric methane
771 lifetime compares well to the trend in the atmospheric methane lifetime from the CMAM
772 model. Both anthropogenic emissions and methane concentration during the early part of the
773 1850-2008 historical period are more uncertain than during the later part and therefore the
774 differences between simulated and observation-based estimates of atmospheric methane
775 concentration (in Figure 9a) and methane lifetimes (in Figure 9b) for the period 1850-1900
776 are not unexpected.

777

778 While the results in Figures 9a and 9b provide some confidence that the magnitude and
779 temporal evolution of simulated global natural methane sources and sinks over the historical
780 period are reasonable they, of course, do not allow the evaluation of all of the simulated
781 natural fluxes individually.

782

783 We also evaluate the role of increase in wetland methane emissions over the historical period
784 (as seen in Figure 6) on the historical methane budget. Instead of using wetland methane
785 emissions from the transient historical simulation in the one box model of atmospheric
786 methane we use wetland methane emissions from the equilibrium pre-industrial simulation in
787 which 1901-1925 CRU-NCEP meteorological data are used repeatedly and CO₂ is held
788 constant at its pre-industrial level of 285 ppm. As a result wetland extent and methane
789 emissions do not respond to changes in climate and increasing CO₂, and do not increase over
790 the historical period (as seen in Figure 10a). Methane emissions from fire and soil uptake of
791 methane still respond to changes in climate and increasing CO₂. The result of using these



792 wetland methane emissions (shown in Figure 10a) in the framework of the one box model of
793 atmospheric methane is shown in Figure 10b. In Figure 10b, although [CH₄] overall increases
794 over the historical period in response to increase in anthropogenic emissions, the result of
795 wetland methane emissions not increasing over the historical period is that the simulated
796 atmospheric methane concentration in year 2008 is calculated to be 1685 ppm, which is 130
797 ppb lower than the 1815 ppb seen in Figure 9a.

798

799 3.3 Geographical distribution of wetland extent

800

801 Figure 11 compares the zonally-averaged maximum wetland fraction over land with
802 observation-based estimates based on the Global Lakes and Wetland (GLWD; Lehner and
803 Döll, 2004) and the new product formed by merging remote sensing based observations of
804 daily surface inundation from the Surface Water Microwave Product Series (SWAMPS;
805 Schroeder et al., 2015) with the static inventory of wetland area from the GLWD from
806 Poulter et al. (2017), as mentioned earlier in section 2.1.3. Maximum wetland fraction from
807 the model and SWAMPS+GLWD product is calculated as the maximum of 12 mean monthly
808 values from the 13 years spanning the 2000-2012 period. Figure 11 shows that overall the
809 model is able to capture the broad latitudinal distribution of wetlands with higher wetland
810 fraction at northern high-latitudes and in the tropics. The model yields higher wetland
811 fraction in the tropics than both observation-based estimates and this is due to higher wetland
812 fraction simulated in the Amazonian region. The Amazonian region is densely forested and
813 the SWAMPS product is unable to map wetlands beneath closed forest canopies. Biases also
814 likely exist in the GLWD data set since parts of the Amazonian region are fairly remote. This
815 is shown in Figure 12 which compares the geographical distribution of simulated maximum
816 wetland fraction with that from the GLWD and SWAMPS+GLWD products. The model



817 successfully captures wetlands in the Hudson Bay lowlands, the West Siberian lowlands, the
818 Pantanal and the region bordering Argentina, Paraguay and Uruguay in South America,
819 Indonesia and the low lying region around Bangladesh. In terms of differences from these
820 observation-based data sets the model most notably overestimates wetland extent in Europe.
821 One possible reason for this is that wetlands in Europe have been drained for agriculture and
822 our wetland parameterization does not take this into account. About two-thirds of the
823 European wetlands that existed 100 years ago have been lost (European Commission, 1995)
824 leading to a substantial decrease in the number and size of large bogs and marshes, and small
825 or shallow lakes.

826

827 **3.4 Geographical distribution of simulated natural fluxes**

828

829 Figure 13 shows the geographical distribution of methane emissions from dynamic wetlands
830 (panel a) and fire (panel b) and the soil uptake of methane (panel c) simulated by the CLASS-
831 CTEM model. The figures also show the global total of these fluxes averaged over the 2000-
832 2008 period for later comparison with estimates from Saunois et al. (2016). Methane
833 emissions from wetlands (168.9 Tg CH₄/yr) are the largest of natural fluxes, as is well
834 known, while emissions from fire (26.8 Tg CH₄/yr) and methane uptake by soil (28.7 Tg
835 CH₄/yr) are an order of magnitude lower. As expected, the geographical distribution of
836 methane emissions from wetlands (Figure 13a) corresponds well to the geographical
837 distribution of wetlands themselves (Figure 12a) although per unit wetland area methane
838 emissions are higher in tropics and milder temperate regions than in high-latitude regions.
839 This is because warmer temperatures and longer growing season in the tropical and milder
840 temperate regions imply that wetlands can emit more methane per unit wetland area and for a
841 longer period of time than the colder high-latitude regions with a shorter growing season. In



842 Figure 13b the geographical distribution of methane fire emissions shows higher values in
843 seasonally-dry tropical regions and order of magnitudes lower values in mid-high latitude
844 regions. These results are consistent with area burned (not shown) which shows a similar
845 pattern. Finally, the geographical distribution of methane uptake by soils in Figure 13c shows
846 higher methane uptake by soils in parts of dry regions (including the Sahara and the
847 Australian outback) where soil moisture doesn't get too dry (so as to not excessively limit
848 soil microbial activity) but otherwise fairly uniform uptake in the tropics and lower values in
849 mid-high latitude regions where lower temperatures and higher soil moisture limit methane
850 uptake by soils.

851

852 **3.5 Regional evaluation over West Siberia lowlands**

853

854 While evaluation of simulated global wetland extent and wetland methane emissions, and
855 their geographical distribution, provides confidence in model results, we further evaluate the
856 model at a regional scale over the West Siberia lowlands. The model results are sampled for
857 the region lying between 50 to 75 °N and 60 to 95°E for comparison with observation- and
858 inversion-based estimates (mentioned earlier in section 2.1.3). Figure 14a compares CLASS-
859 CTEM simulated wetland extent with those from models participating in the WETCHIMP-
860 WSL intercomparison, and the GIEMS, SWAMPS and merged SWAMPS and GLWD
861 products mentioned in section 2.1.3. Table 3 compares the simulated annual maximum
862 wetland extent with models participating in the WETCHIMP-WSL intercomparison and these
863 observation-based products. All values are reported as average for the period 1993-2004
864 except for the merged SWAMPS and GLWD product whose average is for the 2002-2012
865 period, and the Peregon et al. (2009) estimate that is based on wetland typology map from a
866 1977 publication and a more recent satellite land cover product. CLASS-CTEM simulated
867 monthly wetland extent in Figure 14a compares best with the merged SWAMPS and GLWD



868 product, while both the satellite-based inundation products by themselves (SWAMPS and
869 GIEMS) show much lower values. Satellite-based products that remotely sense inundated
870 areas can only do so when water table is above the ground and therefore wetland areas
871 inferred from these products are expected to be lower in magnitude than products which also
872 take into account land cover as is the case for the merged SWAMPS and GLWD product.

873

874 In Table 3, the annual maximum wetland extent is quite similar for the merged SWAMPS
875 and GLWD product (0.55 million km²) and CLASS-CTEM simulated values (0.53 million
876 km²) but the maximum occurs in different months. In Figure 14b, for the merged SWAMPS
877 and GLWD product the maximum wetland extent occurs in June while CLASS-CTEM
878 simulated values show peak both in June and September. The participating models from the
879 WETCHIMP-WSL intercomparison show a range of values for the monthly wetland extent in
880 the WSL region (Figure 14a). Models range from those which specify constant values with
881 no seasonality for the wetland extent to models which dynamically model wetland extent two
882 of which show maximum wetland extent of greater than 1 million km². The average annual
883 maximum wetland extent across the participating models in the WETCHIMP-WSL is
884 0.70±0.15 million km² (mean ± standard error). Finally, the Pregon et al. (2009) estimate is
885 0.68 million km² which is somewhat higher than the CLASS-CTEM simulated value (0.53
886 million km²) and the merged SWAMPS and GLWD product (0.55 million km²).

887

888 Figure 14b compares CLASS-CTEM simulated monthly wetland methane emissions with
889 those from models participating in the WETCHIMP-WSL intercomparison and four
890 inversion-based estimates mentioned in section 2.1.3. The two Bousquet et al. (2011)
891 inversions shown in Figure 14b correspond to ones using the reference Matthews and Fung
892 (1987) emissions inventory (Bousquet 2001 R) and the emissions inventory based on Kaplan



893 (2002) (Bousquet 2001 K). All values are reported as average for the period 1993-2004
894 except for the Kim et al. (2011) inversion which reports fluxes for year 2005 and the
895 Winderlich (2012) inversion which corresponds to year 2009.

896

897 Table 3 compares the simulated annual wetland methane emissions from CLASS_CTEM
898 with those from models participating in the WETCHIMP-WSL intercomparison and the four
899 inversion-based estimates. In Table 3, the inversion-based annual wetland methane emissions
900 vary from 3.08 to 9.80 Tg CH₄/yr. The highest annual emissions in the Winderlich (2012)
901 inversion are due to higher emissions in the shoulder months of spring and fall compared to
902 other inversions but also non-zero emissions during winter months (December to February)
903 as seen in Figure 14b. The CLASS-CTEM model calculates annual wetland methane
904 emissions of 7.76 Tg CH₄/yr and the average for models participating in the WETCHIMP-
905 WSL intercomparison is 5.34±0.54 Tg CH₄/yr (mean ± standard error). Of all the models and
906 inversions only the Winderlich (2012) inversion shows substantial methane emissions for the
907 November to April period. In CLASS-CTEM as the liquid soil moisture in the top soil layer
908 freezes wetland extent contracts to zero (Figure 14a) and methane emissions are shut off
909 during the winter months. Bohn et al. (2015) note that Winderlich (2012) inversion-based
910 estimates may have been influenced by emissions from fossil fuel extraction and biomass
911 burning, although the seasonality of Winderlich (2012) fluxes, with non-zero emissions even
912 in winter, is plausible. Based on year-round eddy flux measurements of methane emissions
913 from an Alaskan Arctic tundra sites Zona et al. (2016) find that cold season (September to
914 May) emissions account for ≥50% of the annual methane flux, with the highest emissions
915 from non-inundated upland tundra. They find a major fraction of cold season emissions occur
916 during the “zero curtain” period, when subsurface soil temperatures are near 0 °C. So it is



917 entirely plausible that methane emissions occur during winter months which models fail to
918 simulate and most inversions fail to capture.

919

920 **3.6 Evaluation of present-day global methane budget**

921

922 Our final evaluation of simulated global methane budget is against estimates compiled by
923 Saunois et al. (2016) who synthesize several recent studies to summarize the present-day
924 global methane budget. Our global methane budget is based on simulated and specified fluxes
925 and the use of one box model of atmospheric methane. We exclusively evaluate our
926 simulated global methane budget against the top-down approaches presented in Saunois et al.
927 (2016) since estimates from bottom-up approaches are known to yield higher total emissions
928 than those based on top-down approaches as mentioned earlier in the Introduction. The global
929 methane budget based on top-down approaches which are constrained by the atmospheric
930 CH₄ burden and its loss in the atmosphere is considered more reliable than that based on the
931 bottom-up approaches. These comparisons are shown in Table 4. The natural and
932 anthropogenic sources are divided into their broad categories and so are the sinks which are
933 divided into atmospheric and soil sinks. The Saunois et al. (2016) estimates are reported for
934 the period 2000-2009 while the CLASS-CTEM values correspond to the 2000-2008 period
935 since the EDGAR anthropogenic emissions were available only until 2008 at the time of this
936 study and therefore the one box model of atmospheric methane is also run up until 2008. For
937 clarity, Table 4 also identifies which fluxes are modelled by CLASS-CTEM, which are
938 specified and which are based on atmospheric methane lifetimes.

939

940 In Table 4 the total emissions from natural sources in our framework are 199 Tg CH₄/yr
941 which are in the lower part of the range of 194-292 Tg CH₄/yr compiled by Saunois et al.



942 (2016). This is due to lower specified emissions from non-wetland sources. While our
943 modelled emissions from wetlands of 169 Tg CH₄/yr compare well with the Saunois et al.
944 (2016) central estimate of 166 Tg CH₄/yr, our specified emissions from other natural sources
945 (including termites, geological sources and fresh water bodies) of 30 Tg CH₄/yr are near the
946 low end of their range (21-130 Tg CH₄/yr). In contrast, our anthropogenic emissions of 344
947 Tg CH₄/yr (which include emissions from fire for consistency with Saunois et al. (2016)) are
948 higher than Saunois et al. (2016) central estimate of 319 Tg CH₄/yr and towards the higher
949 end of their range (255-357 Tg CH₄/yr). This is due to the use of EDGAR emissions which as
950 Saunois et al. (2016) note are towards the higher end of all data sets of anthropogenic
951 emissions. Our modelled fire emissions of 27 Tg CH₄/yr are lower than Saunois et al. (2016)
952 central estimate of 35 Tg CH₄/yr. One reason for this is that while we include natural and
953 anthropogenic fires in our framework we do not account for biofuel burning. Overall, our
954 emissions from natural sources are 35 Tg CH₄/yr lower, and emissions from anthropogenic
955 sources are 25 Tg CH₄/yr higher, than the Saunois et al. (2016) central estimates. As a result,
956 the sum of natural and anthropogenic emissions (543 Tg CH₄/yr) in our framework is 9 Tg
957 CH₄/yr lower than Saunois et al. (2016) central estimate (552 Tg CH₄/yr).

958

959 The total sink strength is calculated to be 538 Tg CH₄/yr in our framework which compares
960 well with the Saunois et al. (2016) estimate of 546 Tg CH₄/yr. Saunois et al. (2016) do not
961 provide uncertainty ranges for the atmospheric and total sink. The modelled atmospheric (509
962 Tg CH₄/yr) and soil (29 Tg CH₄/yr) sinks in Table 4 also compare well with Saunois et al.
963 (2016) estimates of 514 and 32 Tg CH₄/yr, respectively.

964

965 **4. Discussion and conclusions**

966



967 The offline evaluation of natural methane fluxes simulated by the CLASS-CTEM modelling
968 framework presented here is the first step in making atmospheric methane concentration a
969 prognostic variable in the family of Canadian earth system models. The evaluation is based
970 on comparison of present-day fluxes with existing observation- and model-based estimates
971 compiled by Saunio et al. (2016) but also the historical evolution of atmospheric methane
972 burden and methane's lifetime simulated using a one box model of atmospheric methane.
973 While our simulated and specified present-day global methane budget components lie within
974 the uncertainty range for top-down estimates from Saunio et al. (2016) this uncertainty range
975 also implies that methane emissions from individual sectors for the present-day budget can be
976 increased or decreased within their uncertainty ranges as long as the total emissions stay the
977 same. The time evolution of the atmospheric methane burden over the historical period,
978 however, provides additional constraints than the present-day methane budget. For example,
979 our specified methane emissions of 30 Tg CH₄/yr from other nature sources (E_o) (including
980 termites, geological sources, wild animals and freshwater) are lower than Saunio et al.
981 (2016) central estimate of 68 Tg CH₄/yr, although still within their uncertainty range. In the
982 absence of any information about its time evolution we have assumed that E_o remains
983 constant over the historical period. This is a plausible assumption since we do not expect
984 emissions from termites, geological sources, wild animals and freshwater to show a large
985 response to changing environmental conditions over the historical period. Certainly, not as
986 large as we saw for wetland emissions which increased by 40 Tg CH₄/yr over the 1850-2008
987 period (Figure 6). However, when we use a constant E_o of 68 Tg CH₄/yr in our framework
988 we obtain higher than observed methane concentration throughout the historical period and
989 the year 2008 value is 1953 ppb compared to 1815 ppb that we obtain in Figure 9a (observed
990 methane concentration for 2008 is 1790 ppb). This is shown in Figure 15. Part of the reason
991 for this may be that present-day EDGAR emissions are higher than other estimates as Saunio



992 et al. (2016) note and that's why we had to choose a lower E_o . However, the global
993 harmonized and RCP anthropogenic emissions are fairly similar up until 1990 (see Figure 4a)
994 and therefore had we use RCP based emissions (up until year 2000) we still would have
995 obtained higher than observed atmospheric methane concentrations throughout the historical
996 period when using E_o of 68 Tg CH₄/yr. Our framework cannot accommodate E_o larger than
997 about 30-35 Tg CH₄/yr without over estimating atmospheric methane concentrations
998 throughout the historical period.

999

1000 The second constraint provided by the time evolution of the atmospheric methane burden
1001 over the historical period is that related to wetland methane emissions. As seen in section 3.2,
1002 in the absence of the simulated increase in wetland methane emissions from about 130 to 170
1003 Tg CH₄/yr from 1850s to the present day the simulated year 2008 atmospheric methane
1004 concentration is about 100 ppb lower than observed (as seen in Figure 10). Assuming our
1005 RCP and EDGAR based harmonized anthropogenic emissions and their increase over the
1006 historical period is reasonably realistic, this indicates that it is very likely that wetland
1007 methane emissions have indeed increased over the historical period in response to changes in
1008 climate and increased atmospheric CO₂ concentration. The results in section 3.1 showed that
1009 this increase of 30% in wetland methane emissions is driven more by an increase in methane
1010 emissions per unit area than the increase in maximum wetland extent, which increased by
1011 about 8% over the historical period. The implication of this is that wetland methane
1012 emissions will likely keep increasing in the future in response to the increasing atmospheric
1013 concentration of CO₂ driven by higher heterotrophic respiration.

1014

1015 The evaluation of simulated wetland extent against the GLWD and the merged SWAMPS
1016 and GLWD product provides confidence that the model is broadly able to reproduce the



1017 geographical distribution of wetlands although, of course, some limitations remain. Over the
1018 WSL region the simulated estimates of wetland extent and wetland methane emissions are
1019 also broadly consistent with observation-based estimates.

1020

1021 We have not evaluated the model's wetland methane emissions at the site level against
1022 observations. Wetland methane emissions are known to be spatially highly heterogeneous and
1023 temporally intermittent (e.g. Godwin et al., 2013) and CLASS-CTEM does not represent
1024 physical processes that govern methane emissions at small spatial and temporal scales.
1025 Instead the model is designed for operation at large spatial scales (> 100 km) and
1026 implementation within an Earth system model and as such only temperature, soil moisture
1027 and substrate availability (through heterotrophic respiration) are taken into account. Water
1028 table depth, ebullition, and transport through vascular plants are not considered in our
1029 modelling framework. Similar approaches are followed by several large scale models
1030 including a recent attempt by Bloom et al. (2017) who derive wetland methane emissions
1031 using heterotrophic respiration from eight terrestrial ecosystem models.

1032

1033 Our next step to evaluate natural methane fluxes from CLASS-CTEM is to use these fluxes in
1034 an atmospheric transport model to simulate and compare methane concentrations at selected
1035 stations. In addition, CLASS-CTEM simulated fluxes can be used as a prior in a methane
1036 inversion-based system to calculate optimized posterior fluxes to which the prior fluxes can
1037 be compared. Although atmospheric inversions-based systems have their own limitations
1038 (Houweling et al., 2017), the objective is to evaluate CLASS-CTEM simulated natural
1039 methane fluxes using a range of available methodologies.

1040



1041 Overall the results presented here suggest that the natural fluxes of methane between the
1042 atmosphere and the land, and the geographical distribution of wetland extent, simulated by
1043 the CLASS-CTEM modelling framework are sufficiently realistic to use the model to study
1044 the changes in natural methane fluxes due to changes in environmental conditions.

1045

1046

1047 **Acknowledgements**

1048

1049 We would like to thank Douglas Chan and Reinel Sospedra-Alfonso for providing comments
1050 on an earlier version of this manuscript.

1051

1052

1053 **References**

- 1054 Amante, C. and Eakins, B. W.: ETOPO1 1 Arc-Minute Global Relief Model: Procedures,
1055 Data Sources and Analysis. NOAA Technical Memorandum NESDIS NGDC-24, , 19 pp.,
1056 doi:10.7289/V5C8276M, 2009.
- 1057 Andreae, M. O. and Merlet, P.: Emission of trace gases and aerosols from biomass burning,
1058 *Glob. Biogeochem. Cycles*, 15(4), 955–966, doi:10.1029/2000GB001382, 2001.
- 1059 Arora, V. K.: Land surface modelling in general circulation models: a hydrological
1060 perspective, PhD thesis, University of Melbourne, Melbourne, Australia., 1997.
- 1061 Arora, V. K. and Boer, G. J.: A Representation of Variable Root Distribution in Dynamic
1062 Vegetation Models, *Earth Interact.*, 7(6), 1–19, doi:10.1175/1087-
1063 3562(2003)007<0001:AROV RD>2.0.CO;2, 2003.
- 1064 Arora, V. K. and Boer, G. J.: A parameterization of leaf phenology for the terrestrial
1065 ecosystem component of climate models, *Glob. Change Biol.*, 11(1), 39–59,
1066 doi:10.1111/j.1365-2486.2004.00890.x, 2005a.
- 1067 Arora, V. K. and Boer, G. J.: Fire as an interactive component of dynamic vegetation models,
1068 *J. Geophys. Res. Biogeosciences*, 110(G2), doi:10.1029/2005JG000042, 2005b.
- 1069 Arora, V. K. and Boer, G. J.: Uncertainties in the 20th century carbon budget associated with
1070 land use change, *Glob. Change Biol.*, 16(12), 3327–3348, doi:10.1111/j.1365-
1071 2486.2010.02202.x, 2010.
- 1072 Arora, V. K. and Scinocca, J. F.: Constraining the strength of the terrestrial CO₂ fertilization
1073 effect in the Canadian Earth system model version 4.2 (CanESM4.2), *Geosci. Model Dev.*,
1074 9(7), 2357–2376, doi:10.5194/gmd-9-2357-2016, 2016.
- 1075 Arora, V. K., Boer, G. J., Christian, J. R., Curry, C. L., Denman, K. L., Zahariev, K., Flato, G.
1076 M., Scinocca, J. F., Merryfield, W. J. and Lee, W. G.: The Effect of Terrestrial
1077 Photosynthesis Down Regulation on the Twentieth-Century Carbon Budget Simulated with
1078 the CCCma Earth System Model, *J. Clim.*, 22(22), 6066–6088,
1079 doi:10.1175/2009JCLI3037.1, 2009.
- 1080 Arora, V. K., Scinocca, J. F., Boer, G. J., Christian, J. R., Denman, K. L., Flato, G. M.,
1081 Kharin, V. V., Lee, W. G. and Merryfield, W. J.: Carbon emission limits required to satisfy
1082 future representative concentration pathways of greenhouse gases, *Geophys. Res. Lett.*,
1083 38(5), doi:10.1029/2010GL046270, 2011.
- 1084 Arora, V. K., Boer, G. J., Friedlingstein, P., Eby, M., Jones, C. D., Christian, J. R., Bonan, G.,
1085 Bopp, L., Brovkin, V., Cadule, P., Hajima, T., Ilyina, T., Lindsay, K., Tjiputra, J. F. and Wu,
1086 T.: Carbon–Concentration and Carbon–Climate Feedbacks in CMIP5 Earth System Models,
1087 *J. Clim.*, 26(15), 5289–5314, doi:10.1175/JCLI-D-12-00494.1, 2013.
- 1088 Bloom, A. A., Bowman, K. W., Lee, M., Turner, A. J., Schroeder, R., Worden, J. R., Weidner,
1089 R., McDonald, K. C. and Jacob, D. J.: A global wetland methane emissions and uncertainty
1090 dataset for atmospheric chemical transport models (WetCHARTs version 1.0), *Geosci Model
1091 Dev.*, 10(6), 2141–2156, doi:10.5194/gmd-10-2141-2017, 2017.
- 1092 Bohn, T. J., Melton, J. R., Ito, A., Kleinen, T., Spahni, R., Stocker, B. D., Zhang, B., Zhu, X.,
1093 Schroeder, R., Glagolev, M. V., Maksyutov, S., Brovkin, V., Chen, G., Denisov, S. N.,
1094 Eliseev, A. V., Gallego-Sala, A., McDonald, K. C., Rawlins, M. A., Riley, W. J., Subin, Z. M.,



- 1095 Tian, H., Zhuang, Q. and Kaplan, J. O.: WETCHIMP-WSL: intercomparison of wetland
1096 methane emissions models over West Siberia, *Biogeosciences*, 12(11), 3321–3349,
1097 doi:10.5194/bg-12-3321-2015, 2015.
- 1098 Bousquet, P., Ringeval, B., Pison, I., Dlugokencky, E. J., Brunke, E.-G., Carouge, C.,
1099 Chevallier, F., Fortems-Cheiney, A., Frankenberg, C., Hauglustaine, D. A., Krummel, P. B.,
1100 Langenfelds, R. L., Ramonet, M., Schmidt, M., Steele, L. P., Szopa, S., Yver, C., Viovy, N.
1101 and Ciais, P.: Source attribution of the changes in atmospheric methane for 2006–2008,
1102 *Atmos Chem Phys*, 11(8), 3689–3700, doi:10.5194/acp-11-3689-2011, 2011.
- 1103 Collins, W. J., Bellouin, N., Doutriaux-Boucher, M., Gedney, N., Halloran, P., Hinton, T.,
1104 Hughes, J., Jones, C. D., Joshi, M., Liddicoat, S., Martin, G., O'Connor, F., Rae, J., Senior,
1105 C., Sitch, S., Totterdell, I., Wiltshire, A. and Woodward, S.: Development and evaluation of
1106 an Earth-System model – HadGEM2, *Geosci. Model Dev.*, 4(4), 1051–1075,
1107 doi:10.5194/gmd-4-1051-2011, 2011.
- 1108 Curry, C. L.: Modeling the soil consumption of atmospheric methane at the global scale,
1109 *Glob. Biogeochem. Cycles*, 21(4), doi:10.1029/2006GB002818, 2007.
- 1110 Dalva, M., Moore, T. R., Arp, P. and Clair, T. A.: Methane and soil and plant community
1111 respiration from wetlands, Kejimikujik National Park, Nova Scotia: Measurements,
1112 predictions, and climatic change, *J. Geophys. Res. Atmospheres*, 106(D3), 2955–2962,
1113 doi:10.1029/2000JD900500, 2001.
- 1114 Denman, K. L., Brasseur, G., Chidthaisong, A., Ciais, P., Cox, P. M., Dickinson, R. E.,
1115 Hauglustaine, D., Heinze, C., Holland, E., Jacob, D., Lohmann, U., Ramachandran, S., da
1116 Silva Dias, P. L., Wofsy, S. C. and Zhang, H.: Couplings Between Changes in the Climate
1117 System and Biogeochemistry, in *Climate Change 2007: The Physical Science Basis*.
1118 Contribution of Working Group I to the Fourth Assessment Report of the Intergovernmental
1119 Panel on Climate Change [Solomon, S., D. Qin, M. Manning, Z. Chen, M. Marquis, K.B.
1120 Averyt, M. Tignor and H.L. Miller (eds.)], pp. 499–587, Cambridge University Press,
1121 Cambridge, United Kingdom and New York, NY, USA., 2007.
- 1122 European Commission: Wise use and conservation of wetlands. Communication from the
1123 Commission to the Council and the European Parliament, European Commission, Brussels,
1124 Belgium. [online] Available from: <http://aei.pitt.edu/4792/1/4792.pdf> (Accessed 12 September
1125 2017), 1995.
- 1126 Eyring, V., Butchart, N., Waugh, D. W., Akiyoshi, H., Austin, J., Bekki, S., Bodeker, G. E.,
1127 Boville, B. A., Brühl, C., Chipperfield, M. P., Cordero, E., Dameris, M., Deushi, M., Fioletov,
1128 V. E., Frith, S. M., Garcia, R. R., Gettelman, A., Giorgetta, M. A., Grewe, V., Jourdain, L.,
1129 Kinnison, D. E., Mancini, E., Manzini, E., Marchand, M., Marsh, D. R., Nagashima, T.,
1130 Newman, P. A., Nielsen, J. E., Pawson, S., Pitari, G., Plummer, D. A., Rozanov, E.,
1131 Schraner, M., Shepherd, T. G., Shibata, K., Stolarski, R. S., Struthers, H., Tian, W. and
1132 Yoshiki, M.: Assessment of temperature, trace species, and ozone in chemistry-climate
1133 model simulations of the recent past, *J. Geophys. Res. Atmospheres*, 111(D22), n/a-n/a,
1134 doi:10.1029/2006JD007327, 2006.
- 1135 Friedlingstein, P., Cox, P., Betts, R., Bopp, L., von Bloh, W., Brovkin, V., Cadule, P., Doney,
1136 S., Eby, M., Fung, I., Bala, G., John, J., Jones, C., Joos, F., Kato, T., Kawamiya, M., Knorr,
1137 W., Lindsay, K., Matthews, H. D., Raddatz, T., Rayner, P., Reick, C., Roeckner, E.,
1138 Schnitzler, K.-G., Schnur, R., Strassmann, K., Weaver, A. J., Yoshikawa, C. and Zeng, N.:
1139 Climate–Carbon Cycle Feedback Analysis: Results from the C4MIP Model Intercomparison,
1140 *J. Clim.*, 19(14), 3337–3353, doi:10.1175/JCLI3800.1, 2006.



- 1141 Friedlingstein, P., Meinshausen, M., Arora, V. K., Jones, C. D., Anav, A., Liddicoat, S. K. and
1142 Knutti, R.: Uncertainties in CMIP5 Climate Projections due to Carbon Cycle Feedbacks, *J.*
1143 *Clim.*, 27(2), 511–526, doi:10.1175/JCLI-D-12-00579.1, 2014.
- 1144 Giglio, L., Randerson, J. T. and van der Werf, G. R.: Analysis of daily, monthly, and annual
1145 burned area using the fourth-generation global fire emissions database (GFED4), *J.*
1146 *Geophys. Res. Biogeosciences*, 118(1), 317–328, doi:10.1002/jgrg.20042, 2013.
- 1147 Glagolev, M. V., Kleptsova, I. E., Filippov, I. V., Kazantsev, V. S., Machida, T. and
1148 Maksyutov, S. S.: Methane emissions from subtaiga mires of Western Siberia: The “standard
1149 model” Bc5, *Mosc. Univ. Soil Sci. Bull.*, 65(2), 86–93, doi:10.3103/S0147687410020067,
1150 2010.
- 1151 Godwin, C. M., McNamara, P. J. and Markfort, C. D.: Evening methane emission pulses
1152 from a boreal wetland correspond to convective mixing in hollows, *J. Geophys. Res.*
1153 *Biogeosciences*, 118(3), 994–1005, doi:10.1002/jgrg.20082, 2013.
- 1154 Houweling, S., Bergamaschi, P., Chevallier, F., Heimann, M., Kaminski, T., Krol, M.,
1155 Michalak, A. M. and Patra, P.: Global inverse modeling of CH₄ sources and sinks: an
1156 overview of methods, *Atmos Chem Phys*, 17(1), 235–256, doi:10.5194/acp-17-235-2017,
1157 2017.
- 1158 Hurtt, G. C., Frolking, S., Fearon, M. G., Moore, B., Shevliakova, E., Malyshev, S., Pacala,
1159 S. W. and Houghton, R. A.: The underpinnings of land-use history: three centuries of global
1160 gridded land-use transitions, wood-harvest activity, and resulting secondary lands, *Glob.*
1161 *Change Biol.*, 12(7), 1208–1229, doi:10.1111/j.1365-2486.2006.01150.x, 2006.
- 1162 Jones, C., Robertson, E., Arora, V., Friedlingstein, P., Shevliakova, E., Bopp, L., Brovkin, V.,
1163 Hajima, T., Kato, E., Kawamiya, M., Liddicoat, S., Lindsay, K., Reick, C. H., Roelandt, C.,
1164 Segschneider, J. and Tjiputra, J.: Twenty-First-Century Compatible CO₂ Emissions and
1165 Airborne Fraction Simulated by CMIP5 Earth System Models under Four Representative
1166 Concentration Pathways, *J. Clim.*, 26(13), 4398–4413, doi:10.1175/JCLI-D-12-00554.1,
1167 2013.
- 1168 Kaplan, J. O.: Wetlands at the Last Glacial Maximum: Distribution and methane emissions,
1169 *Geophys. Res. Lett.*, 29(6), 3–1, doi:10.1029/2001GL013366, 2002.
- 1170 Kim, H.-S., Maksyutov, S., Glagolev, M. V., Machida, T., Patra, P. K., Sudo, K. and Inoue,
1171 G.: Evaluation of methane emissions from West Siberian wetlands based on inverse
1172 modeling, *Environ. Res. Lett.*, 6(3), 035201, 2011.
- 1173 Kloster, S., Mahowald, N. M., Randerson, J. T., Thornton, P. E., Hoffman, F. M., Levis, S.,
1174 Lawrence, P. J., Feddema, J. J., Oleson, K. W. and Lawrence, D. M.: Fire dynamics during
1175 the 20th century simulated by the Community Land Model, *Biogeosciences*, 7(6), 1877–
1176 1902, doi:10.5194/bg-7-1877-2010, 2010.
- 1177 Lamarque, J.-F., Bond, T. C., Eyring, V., Granier, C., Heil, A., Klimont, Z., Lee, D., Lioussé,
1178 C., Mieville, A., Owen, B., Schultz, M. G., Shindell, D., Smith, S. J., Stehfest, E., Van
1179 Aardenne, J., Cooper, O. R., Kainuma, M., Mahowald, N., McConnell, J. R., Naik, V., Riahi,
1180 K. and van Vuuren, D. P.: Historical (1850–2000) gridded anthropogenic and biomass
1181 burning emissions of reactive gases and aerosols: methodology and application,
1182 *Atmospheric Chem. Phys.*, 10(15), 7017–7039, doi:10.5194/acp-10-7017-2010, 2010.
- 1183 Lamarque, J.-F., Shindell, D. T., Josse, B., Young, P. J., Cionni, I., Eyring, V., Bergmann, D.,
1184 Cameron-Smith, P., Collins, W. J., Doherty, R., Dalsoren, S., Faluvegi, G., Folberth, G.,



- 1185 Ghan, S. J., Horowitz, L. W., Lee, Y. H., MacKenzie, I. A., Nagashima, T., Naik, V.,
1186 Plummer, D., Righi, M., Rumbold, S. T., Schulz, M., Skeie, R. B., Stevenson, D. S., Strode,
1187 S., Sudo, K., Szopa, S., Voulgarakis, A. and Zeng, G.: The Atmospheric Chemistry and
1188 Climate Model Intercomparison Project (ACCMIP): overview and description of models,
1189 simulations and climate diagnostics, *Geosci. Model Dev.*, 6(1), 179–206, doi:10.5194/gmd-6-
1190 179-2013, 2013.
- 1191 Lehner, B. and Döll, P.: Development and validation of a global database of lakes, reservoirs
1192 and wetlands, *J. Hydrol.*, 296(1–4), 1–22, doi:10.1016/j.jhydrol.2004.03.028, 2004.
- 1193 Li, F., Zeng, X. D. and Levis, S.: A process-based fire parameterization of intermediate
1194 complexity in a Dynamic Global Vegetation Model, *Biogeosciences Discuss.*, 9(3), 3233–
1195 3287, doi:10.5194/bgd-9-3233-2012, 2012.
- 1196 Marlon, J. R., Bartlein, P. J., Carcaillet, C., Gavin, D. G., Harrison, S. P., Higuera, P. E.,
1197 Joos, F., Power, M. J. and Prentice, I. C.: Climate and human influences on global biomass
1198 burning over the past two millennia, *Nat. Geosci.*, 1(10), 697–702, doi:10.1038/ngeo313,
1199 2008.
- 1200 Matthes, K., Funke, B., Andersson, M. E., Barnard, L., Beer, J., Charbonneau, P., Clilverd,
1201 M. A., Dudok de Wit, T., Haberleiter, M., Hendry, A., Jackman, C. H., Kretzschmar, M.,
1202 Kruschke, T., Kunze, M., Langematz, U., Marsh, D. R., Maycock, A. C., Misios, S., Rodger,
1203 C. J., Scaife, A. A., Seppälä, A., Shangguan, M., Sinnhuber, M., Tourpali, K., Usoskin, I., van
1204 de Kamp, M., Verronen, P. T. and Versick, S.: Solar forcing for CMIP6 (v3.2), *Geosci. Model
1205 Dev.*, 10(6), 2247–2302, doi:10.5194/gmd-10-2247-2017, 2017.
- 1206 Matthews, E. and Fung, I.: Methane emission from natural wetlands: Global distribution,
1207 area, and environmental characteristics of sources, *Glob. Biogeochem. Cycles*, 1(1), 61–86,
1208 doi:10.1029/GB001i001p00061, 1987.
- 1209 Meinshausen, M., Smith, S. J., Calvin, K., Daniel, J. S., Kainuma, M. L. T., Lamarque, J.-F.,
1210 Matsumoto, K., Montzka, S. A., Raper, S. C. B., Riahi, K., Thomson, A., Velders, G. J. M.
1211 and van Vuuren, D. P. P.: The RCP greenhouse gas concentrations and their extensions
1212 from 1765 to 2300, *Clim. Change*, 109(1), 213, doi:10.1007/s10584-011-0156-z, 2011.
- 1213 Melton, J. R. and Arora, V. K.: Competition between plant functional types in the Canadian
1214 Terrestrial Ecosystem Model (CTEM) v. 2.0, *Geosci Model Dev*, 9(1), 323–361,
1215 doi:10.5194/gmd-9-323-2016, 2016.
- 1216 Melton, J. R., Wania, R., Hodson, E. L., Poulter, B., Ringeval, B., Spahni, R., Bohn, T., Avis,
1217 C. A., Beerling, D. J., Chen, G., Eliseev, A. V., Denisov, S. N., Hopcroft, P. O., Lettenmaier,
1218 D. P., Riley, W. J., Singarayer, J. S., Subin, Z. M., Tian, H., Zürcher, S., Brovkin, V., van
1219 Bodegom, P. M., Kleinen, T., Yu, Z. C. and Kaplan, J. O.: Present state of global wetland
1220 extent and wetland methane modelling: conclusions from a model inter-comparison project
1221 (WETCHIMP), *Biogeosciences*, 10(2), 753–788, doi:10.5194/bg-10-753-2013, 2013.
- 1222 Melton, J. R., Shrestha, R. K. and Arora, V. K.: The influence of soils on heterotrophic
1223 respiration exerts a strong control on net ecosystem productivity in seasonally dry
1224 Amazonian forests, *Biogeosciences*, 12(4), 1151–1168, doi:10.5194/bg-12-1151-2015,
1225 2015.
- 1226 Migliavacca, M., Dosio, A., Kloster, S., Ward, D. S., Camia, A., Houborg, R., Houston
1227 Durrant, T., Khabarov, N., Krasovskii, A. A., San Miguel-Ayanz, J. and Cescatti, A.: Modeling
1228 burned area in Europe with the Community Land Model, *J. Geophys. Res. Biogeosciences*,
1229 118(1), 265–279, doi:10.1002/jgrg.20026, 2013.



- 1230 Myhre, G., Shindell, D., Bréon, F.-M., Collins, W., Fuglestedt, J., Huang, J., Koch, D.,
1231 Lamarque, J.-F., Lee, D., Mendoza, B., Nakajima, T., Robock, A., Stephens, G., Takemura,
1232 T. and Zhang, H.: Anthropogenic and Natural Radiative Forcing, in *Climate Change 2013:
1233 The Physical Science Basis. Contribution of Working Group I to the Fifth Assessment Report
1234 of the Intergovernmental Panel on Climate Change*, edited by T. F. Stocker, D. Qin, G.-K.
1235 Plattner, M. Tignor, S. K. Allen, J. Boschung, A. Nauels, Y. Xia, V. Bex, and P. M. Midgley,
1236 pp. 659–740, Cambridge University Press, Cambridge, United Kingdom and New York, NY,
1237 USA., 2013.
- 1238 Naik, V., Voulgarakis, A., Fiore, A. M., Horowitz, L. W., Lamarque, J.-F., Lin, M., Prather, M.
1239 J., Young, P. J., Bergmann, D., Cameron-Smith, P. J., Cionni, I., Collins, W. J., Dalsøren, S.
1240 B., Doherty, R., Eyring, V., Faluvegi, G., Folberth, G. A., Josse, B., Lee, Y. H., MacKenzie, I.
1241 A., Nagashima, T., van Noije, T. P. C., Plummer, D. A., Righi, M., Rumbold, S. T., Skeie, R.,
1242 Shindell, D. T., Stevenson, D. S., Strode, S., Sudo, K., Szopa, S. and Zeng, G.: Preindustrial
1243 to present-day changes in tropospheric hydroxyl radical and methane lifetime from the
1244 Atmospheric Chemistry and Climate Model Intercomparison Project (ACCMIP), *Atmospheric
1245 Chem. Phys.*, 13(10), 5277–5298, doi:10.5194/acp-13-5277-2013, 2013.
- 1246 Neely III, R. R., Conley, A. J., Vitt, F. and Lamarque, J.-F.: A consistent prescription of
1247 stratospheric aerosol for both radiation and chemistry in the Community Earth System Model
1248 (CESM1), *Geosci. Model Dev.*, 9(7), 2459–2470, doi:10.5194/gmd-9-2459-2016, 2016.
- 1249 Papa, F., Prigent, C., Aires, F., Jimenez, C., Rossow, W. B. and Matthews, E.: Interannual
1250 variability of surface water extent at the global scale, 1993–2004, *J. Geophys. Res.*
1251 *Atmospheres*, 115(D12), n/a-n/a, doi:10.1029/2009JD012674, 2010.
- 1252 Peregon, A., Maksyutov, S. and Yamagata, Y.: An image-based inventory of the spatial
1253 structure of West Siberian wetlands, *Environ. Res. Lett.*, 4(4), 045014, 2009.
- 1254 Poulter, B., Bousquet, P., Canadell, J. G., Ciais, P., Peregon, A., Marielle Saunois, Arora, V.
1255 K., Beerling, D. J., Brovkin, V., Jones, C. D., Joos, F., Nicola Gedney, Ito, A., Kleinen, T.,
1256 Koven, C. D., McDonald, K., Melton, J. R., Peng, C., Shushi Peng, Prigent, C., Schroeder,
1257 R., Riley, W. J., Saito, M., Spahni, R., Tian, H., Lyla Taylor, Viovy, N., Wilton, D., Wiltshire,
1258 A., Xu, X., Zhang, B., Zhang, Z. and Zhu, Q.: Global wetland contribution to 2000–2012
1259 atmospheric methane growth rate dynamics, *Environ. Res. Lett.*, 12(9), 094013, 2017.
- 1260 Prather, M. J., Holmes, C. D. and Hsu, J.: Reactive greenhouse gas scenarios: Systematic
1261 exploration of uncertainties and the role of atmospheric chemistry, *Geophys. Res. Lett.*,
1262 39(9), n/a-n/a, doi:10.1029/2012GL051440, 2012.
- 1263 Prigent, C., Papa, F., Aires, F., Rossow, W. B. and Matthews, E.: Global inundation
1264 dynamics inferred from multiple satellite observations, 1993–2000, *J. Geophys. Res.*
1265 *Atmospheres*, 112(D12), n/a-n/a, doi:10.1029/2006JD007847, 2007.
- 1266 Randerson, J. T., Chen, Y., van der Werf, G. R., Rogers, B. M. and Morton, D. C.: Global
1267 burned area and biomass burning emissions from small fires, *J. Geophys. Res.*
1268 *Biogeosciences*, 117(G4), n/a-n/a, doi:10.1029/2012JG002128, 2012.
- 1269 Saunois, M., Bousquet, P., Poulter, B., Peregon, A., Ciais, P., Canadell, J. G., Dlugokencky,
1270 E. J., Etiope, G., Bastviken, D., Houweling, S., Janssens-Maenhout, G., Tubiello, F. N.,
1271 Castaldi, S., Jackson, R. B., Alexe, M., Arora, V. K., Beerling, D. J., Bergamaschi, P., Blake,
1272 D. R., Brailsford, G., Brovkin, V., Bruhwiler, L., Crevoisier, C., Crill, P., Covey, K., Curry, C.,
1273 Frankenberg, C., Gedney, N., Höglund-Isaksson, L., Ishizawa, M., Ito, A., Joos, F., Kim, H.-
1274 S., Kleinen, T., Krummel, P., Lamarque, J.-F., Langenfelds, R., Locatelli, R., Machida, T.,
1275 Maksyutov, S., McDonald, K. C., Marshall, J., Melton, J. R., Morino, I., Naik, V., O'Doherty,



- 1276 S., Parmentier, F.-J. W., Patra, P. K., Peng, C., Peng, S., Peters, G. P., Pison, I., Prigent, C.,
1277 Prinn, R., Ramonet, M., Riley, W. J., Saito, M., Santini, M., Schroeder, R., Simpson, I. J.,
1278 Spahni, R., Steele, P., Takizawa, A., Thornton, B. F., Tian, H., Tohjima, Y., Viovy, N.,
1279 Voulgarakis, A., van Weele, M., van der Werf, G. R., Weiss, R., Wiedinmyer, C., Wilton, D.
1280 J., Wiltshire, A., Worthy, D., Wunch, D., Xu, X., Yoshida, Y., Zhang, B., Zhang, Z. and Zhu,
1281 Q.: The global methane budget 2000–2012, *Earth Syst Sci Data*, 8(2), 697–751,
1282 doi:10.5194/essd-8-697-2016, 2016.
- 1283 Schroeder, R., McDonald, C. K., Chapman, D. B., Jensen, K., Podest, E., Tessler, D. Z.,
1284 Bohn, J. T. and Zimmermann, R.: Development and Evaluation of a Multi-Year Fractional
1285 Surface Water Data Set Derived from Active/Passive Microwave Remote Sensing Data,
1286 *Remote Sens.*, 7(12), doi:10.3390/rs71215843, 2015.
- 1287 Scinocca, J. F., McFarlane, N. A., Lazare, M., Li, J. and Plummer, D.: Technical Note: The
1288 CCCma third generation AGCM and its extension into the middle atmosphere, *Atmospheric*
1289 *Chem. Phys.*, 8(23), 7055–7074, doi:10.5194/acp-8-7055-2008, 2008.
- 1290 Shindell, D., Kuylensstierna, J. C. I., Vignati, E., van Dingenen, R., Amann, M., Klimont, Z.,
1291 Anenberg, S. C., Muller, N., Janssens-Maenhout, G., Raes, F., Schwartz, J., Faluvegi, G.,
1292 Pozzoli, L., Kupiainen, K., Höglund-Isaksson, L., Emberson, L., Streets, D., Ramanathan, V.,
1293 Hicks, K., Oanh, N. T. K., Milly, G., Williams, M., Demkine, V. and Fowler, D.:
1294 Simultaneously Mitigating Near-Term Climate Change and Improving Human Health and
1295 Food Security, *Science*, 335(6065), 183–189, 2012.
- 1296 Shindell, D. T., Pechony, O., Voulgarakis, A., Faluvegi, G., Nazarenko, L., Lamarque, J.-F.,
1297 Bowman, K., Milly, G., Kovari, B., Ruedy, R. and Schmidt, G. A.: Interactive ozone and
1298 methane chemistry in GISS-E2 historical and future climate simulations, *Atmos Chem Phys*,
1299 13(5), 2653–2689, doi:10.5194/acp-13-2653-2013, 2013.
- 1300 SPARC CCMVal: SPARC Report on the Evaluation of Chemistry-Climate Models, V. Eyring,
1301 T. G. Shepherd, D. W. Waugh (Eds.), SPARC Report No. 5, WCRP-132, WMO/TD-No.
1302 1526., 2010.
- 1303 Versegny, D. L.: Class—A Canadian land surface scheme for GCMS. I. Soil model, *Int. J.*
1304 *Climatol.*, 11(2), 111–133, doi:10.1002/joc.3370110202, 1991.
- 1305 Versegny, D. L.: The Canadian land surface scheme (CLASS): Its history and future,
1306 *Atmosphere-Ocean*, 38(1), 1–13, doi:10.1080/07055900.2000.9649637, 2000.
- 1307 Versegny, D. L., McFarlane, N. A. and Lazare, M.: Class—A Canadian land surface scheme
1308 for GCMS, II. Vegetation model and coupled runs, *Int. J. Climatol.*, 13(4), 347–370,
1309 doi:10.1002/joc.3370130402, 1993.
- 1310 Viovy, N.: CRU-NCEP reanalysis data version 4, [online] Available from:
1311 http://dods.extra.cea.fr/store/p529viov/cruncep/V4_1901_2012/, 2012.
- 1312 Voulgarakis, A., Naik, V., Lamarque, J.-F., Shindell, D. T., Young, P. J., Prather, M. J., Wild,
1313 O., Field, R. D., Bergmann, D., Cameron-Smith, P., Cionni, I., Collins, W. J., Dalsøren, S. B.,
1314 Doherty, R. M., Eyring, V., Faluvegi, G., Folberth, G. A., Horowitz, L. W., Josse, B.,
1315 MacKenzie, I. A., Nagashima, T., Plummer, D. A., Righi, M., Rumbold, S. T., Stevenson, D.
1316 S., Strode, S. A., Sudo, K., Szopa, S. and Zeng, G.: Analysis of present day and future OH
1317 and methane lifetime in the ACCMIP simulations, *Atmos Chem Phys*, 13(5), 2563–2587,
1318 doi:10.5194/acp-13-2563-2013, 2013.



- 1319 Walter, B. P. and Heimann, M.: A process-based, climate-sensitive model to derive methane
1320 emissions from natural wetlands: Application to five wetland sites, sensitivity to model
1321 parameters, and climate, *Glob. Biogeochem. Cycles*, 14(3), 745–765,
1322 doi:10.1029/1999GB001204, 2000.
- 1323 Wania, R., Ross, I. and Prentice, I. C.: Implementation and evaluation of a new methane
1324 model within a dynamic global vegetation model: LPJ-WHyMe v1.3.1, *Geosci Model Dev*,
1325 3(2), 565–584, doi:10.5194/gmd-3-565-2010, 2010.
- 1326 Winderlich, J.: Setup of a CO₂ and CH₄ measurement system in Central Siberia and
1327 modeling of its results, Max-Planck-Institut für Biogeochemie, Jena. [online] Available from:
1328 <http://ediss.sub.uni-hamburg.de/volltexte/2012/5533/pdf/Dissertation.pdf>, 2012.
- 1329 Young, P. J., Archibald, A. T., Bowman, K. W., Lamarque, J.-F., Naik, V., Stevenson, D. S.,
1330 Tilmes, S., Voulgarakis, A., Wild, O., Bergmann, D., Cameron-Smith, P., Cionni, I., Collins,
1331 W. J., Dalsøren, S. B., Doherty, R. M., Eyring, V., Faluvegi, G., Horowitz, L. W., Josse, B.,
1332 Lee, Y. H., MacKenzie, I. A., Nagashima, T., Plummer, D. A., Righi, M., Rumbold, S. T.,
1333 Skeie, R. B., Shindell, D. T., Strode, S. A., Sudo, K., Szopa, S. and Zeng, G.: Pre-industrial
1334 to end 21st century projections of tropospheric ozone from the Atmospheric Chemistry and
1335 Climate Model Intercomparison Project (ACCMIP), *Atmospheric Chem. Phys.*, 13(4), 2063–
1336 2090, doi:10.5194/acp-13-2063-2013, 2013.
- 1337 Zhu, Q., Liu, J., Peng, C., Chen, H., Fang, X., Jiang, H., Yang, G., Zhu, D., Wang, W. and
1338 Zhou, X.: Modelling methane emissions from natural wetlands by development and
1339 application of the TRIPLEX-GHG model, *Geosci Model Dev*, 7(3), 981–999,
1340 doi:10.5194/gmd-7-981-2014, 2014a.
- 1341 Zhu, X., Zhuang, Q., Lu, X. and Song, L.: Spatial scale-dependent land–atmospheric
1342 methane exchanges in the northern high latitudes from 1993 to 2004, *Biogeosciences*, 11(7),
1343 1693–1704, doi:10.5194/bg-11-1693-2014, 2014b.
- 1344 Zobler, L.: A World Soil File for Global Climate Modelling, NASA Technical Memorandum
1345 87802, NASA Goddard Institute for Space Studies, New York, USA., 1986.
- 1346 Zona, D., Gioli, B., Commane, R., Lindaas, J., Wofsy, S. C., Miller, C. E., Dinardo, S. J.,
1347 Dengel, S., Sweeney, C., Karion, A., Chang, R. Y.-W., Henderson, J. M., Murphy, P. C.,
1348 Goodrich, J. P., Moreaux, V., Liljedahl, A., Watts, J. D., Kimball, J. S., Lipson, D. A. and
1349 Oechel, W. C.: Cold season emissions dominate the Arctic tundra methane budget, *Proc.*
1350 *Natl. Acad. Sci.*, 113(1), 40–45, 2016.
- 1351
- 1352



1353

1354 **Table 1:** The upper and lower soil wetness thresholds for three latitudinal bands used in
 1355 equation (1) to determine fractional wetland coverage in a given grid cell.

1356

1357

	Latitudinal band		
	40°N to 90°N	35°S to 40°N	90°S to 35°S
w_{low}	0.45	0.55	0.70
w_{high}	0.90	0.99	0.99

1358

1359

1360

1361 **Table 2:** Emissions categories for EDGAR and RCP anthropogenic methane emissions.

1362

EDGAR	RCP
Non-biomass burning categories	
1. Energy manufacturing transformation 2. Non-road transportation 3. Road transportation 4. Residential 5. Fugitive from solid 6. Oil production and refineries 7. Gas production and distribution 8. Industrial processes and product use 9. Enteric fermentation 10. Manure management 11. Agricultural soils 12. Agricultural waste burning 13. Soil waste disposal 14. Waste water 15. Fossil fuel fires	1. Agricultural sector 2. Agricultural waste burning 3. Residential and commercial combustion 4. Energy production and distribution 5. Industrial processes and combustion 6. Land transport emissions 7. Waste treatment and disposal 8. Shipping
Biomass burning categories	
16. Large scale biomass burning	9. Biomass burning from forest fires 10. Biomass burning from grass fires

1363

1364



1365 **Table 3:** Comparison of CLASS-CTEM simulated annual methane emissions and annual
 1366 maximum wetland extent for the West Siberia lowlands (WSL) region with models
 1367 participating in the WETCHIMP-WSL intercomparison and observation- and inversion-based
 1368 estimates as discussed in section 3.5. Numbers shown are mean \pm standard error from Bohn
 1369 et al. (2015) for models participating in the WETCHIMP-WSL intercomparison. Standard
 1370 error is not available for all inversions. All values are reported as average for the period
 1371 1993-2004 unless otherwise noted.
 1372

WSL annual maximum wetland extent (million km ²)	
Model mean from participating models in the WETCHIMP-WSL Intercomparison	0.70 \pm 0.15
CLASS-CTEM (this study)	0.53
GIEMS inundation data set	0.21
SWAMPS inundation data set	0.15
SWAMPS and GCP product (for period 2002-2012)	0.55
Peregon et al. (2009)	0.68
WSL annual wetland emissions (Tg CH ₄ /yr)	
Model mean from participating models in the WETCHIMP-WSL Intercomparison	5.34 \pm 0.54
CLASS-CTEM (this study)	7.76
Bousquet 2011 K	7.06
Bousquet 2011 R	7.13
Kim 2011 (for year 2005)	3.08 \pm 1.40
Winderlich 2012 (for year 2009)	9.80

1373

1374

1375



1376

1377

Table 4: Comparison of the components of the present day methane budget based on this study with those from Saunio et al. (2016) (based on synthesis of published studies). The values used in this study are averaged for the period 2000-2008 (since the last year of the version of EDGAR emissions used is 2008) while Saunio et al. (2016) values correspond to the 2000-2009 period.

1382

1383

	Saunio et al. (2016) estimates based on top-down approaches	Values used in this study and how they were obtained.	
<i>Natural sources</i>	234 [194-292]	199	
Natural wetlands	166 [125-204]	169	CLASS-CTEM simulated
Other natural sources (termites, geological, fresh water etc.)	68 [21-130]	30	Specified as a constant over the historical period
<i>Anthropogenic sources</i>	319 [255-357]	344	
Agriculture and waste	183 [112-241]	200	EDGAR
Fossil fuels	101 [77-126]	117	EDGAR
Biomass and biofuel burning	35 [16-53]	27	CLASS-CTEM simulated
<i>Sum of all sources</i>	552 [535-566]	543	
<i>Sum of all sinks</i>	546	538	
Atmospheric sink	514	509	Based on specified bias-corrected atmospheric CH ₄ lifetimes from CMAM
Soil sink	32 [27-38]	29	CLASS-CTEM simulated

1384

1385

1386

1387

1388

1389

1390

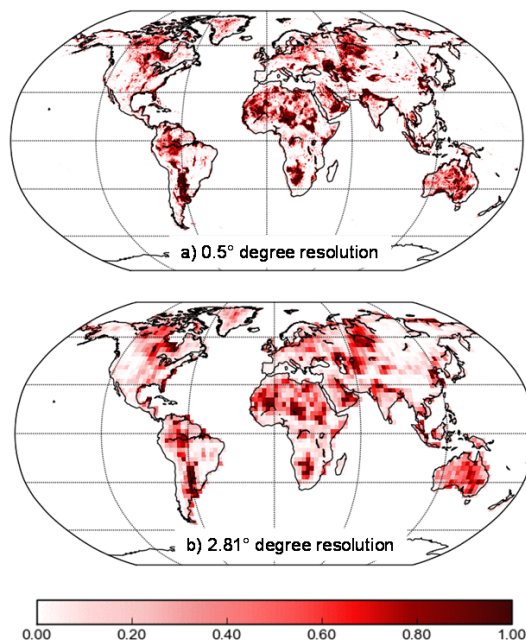


1391

1392

1393

Grid cell fraction with slope < 0.2% which can potentially become a wetland, climate permitting



1394

1395 Figure 1: Fraction of grid cell with slopes less than the threshold of 0.002 (i.e. 0.2% slope) at
1396 a) 0.5° and b) 2.81° spatial resolutions, respectively.

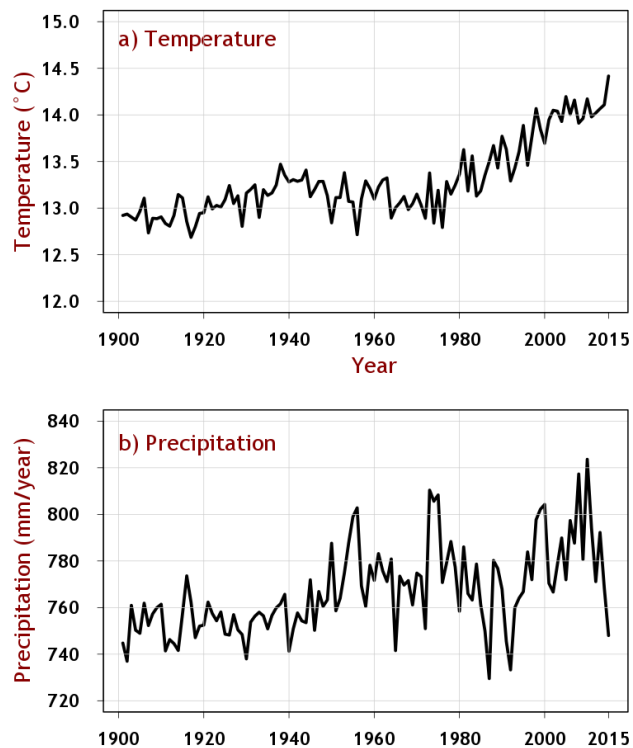
1397

1398



1399

Annual land-averaged temperature and precipitation in CRU-NCEP data (excluding the Antarctica region)



1400

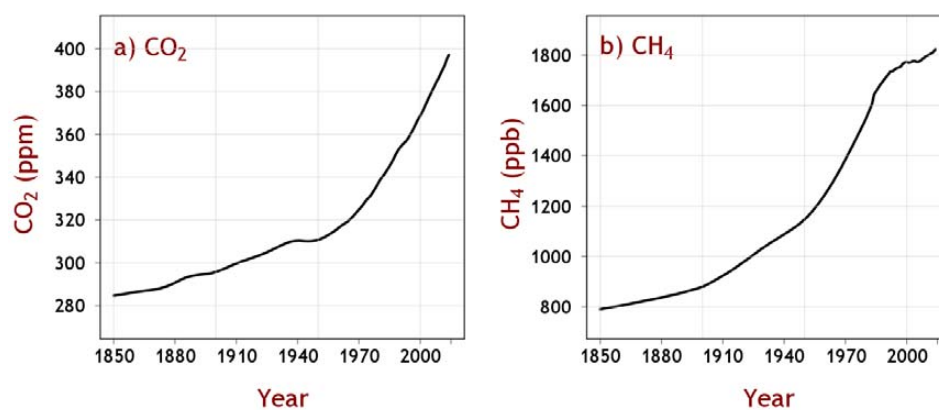
1401 Figure 2: Annual land-averaged temperature and precipitation in version 7 of the CRU-NCEP
1402 data for the period 1901-2015, excluding the Antarctica region, that are used to drive the
1403 CLASS-CTEM model.

1404



1405
1406
1407
1408
1409

Globally-averaged CO₂ and CH₄ concentrations used to drive the CLASS-CTEM model



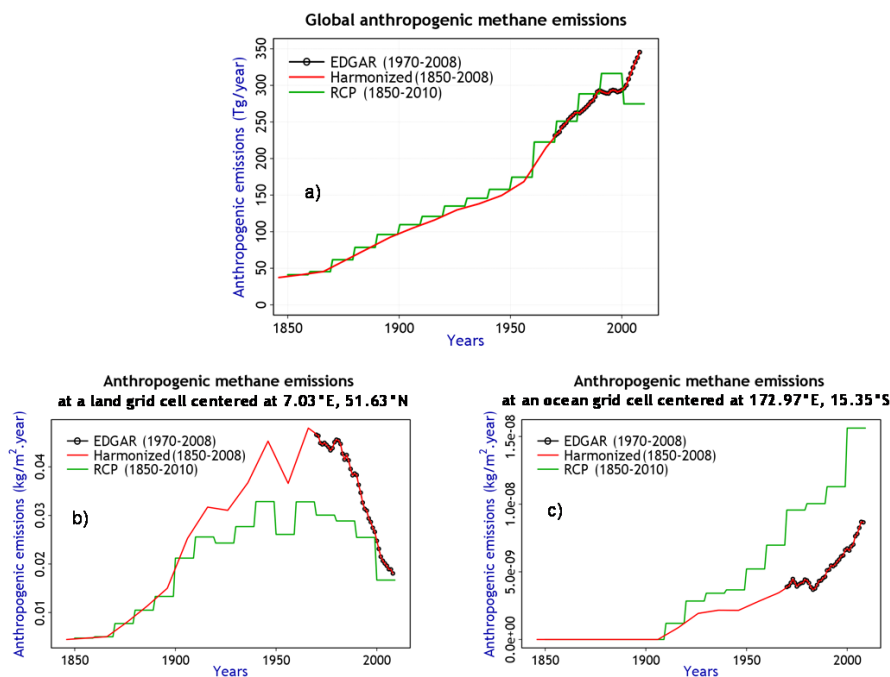
1410
1411
1412
1413
1414
1415

Figure 3: Globally-averaged CO₂ and CH₄ concentrations used to drive the CLASS-CTEM model.



1416

1417



1418

1419 Figure 4: Comparison of RCP, EDGAR and their harmonized annual global anthropogenic
1420 methane emissions (panel a) excluding biomass burning. Panels (b) and (c) illustrate the
1421 harmonization technique for a land and an ocean grid cell, respectively.

1422



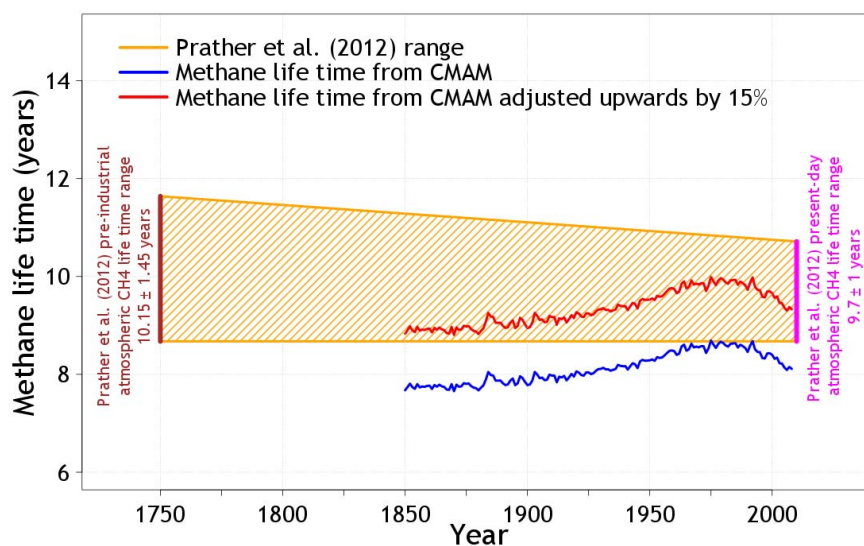
1423

1424

1425

1426

Atmospheric methane life times (excluding the soil sink)



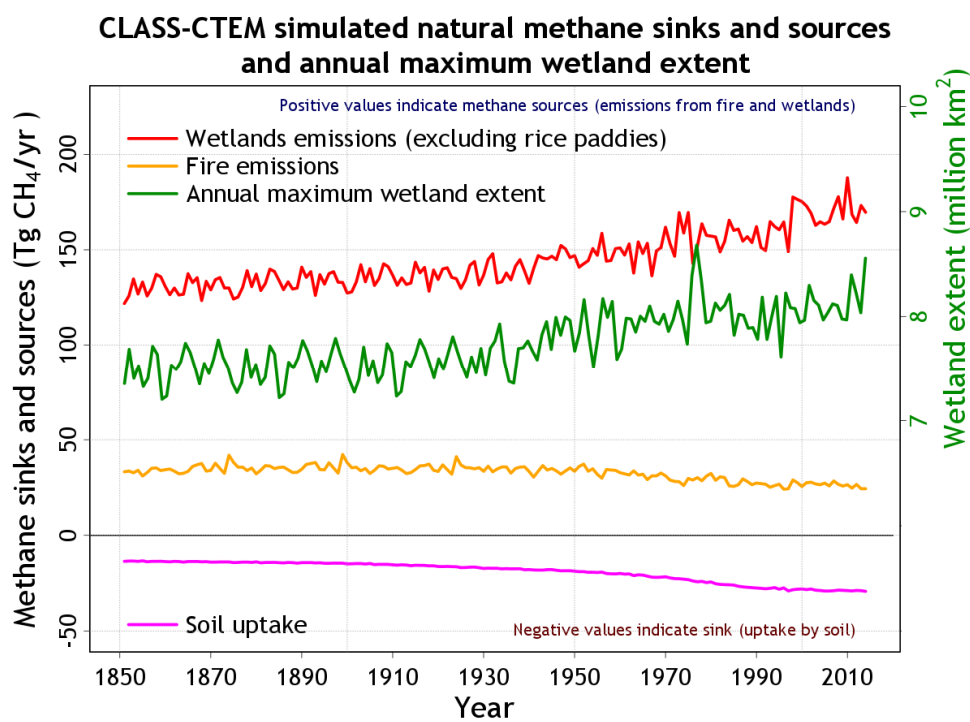
1427

1428 Figure 5: Comparison of atmospheric methane lifetime obtained from the Canadian Middle
1429 Atmosphere Model (CMAM) for the period 1850-2010 with observation-based estimates
1430 from Prather et al. (2012) but excluding the soil sink as explained in section 2.2.3.

1431



1432
1433
1434



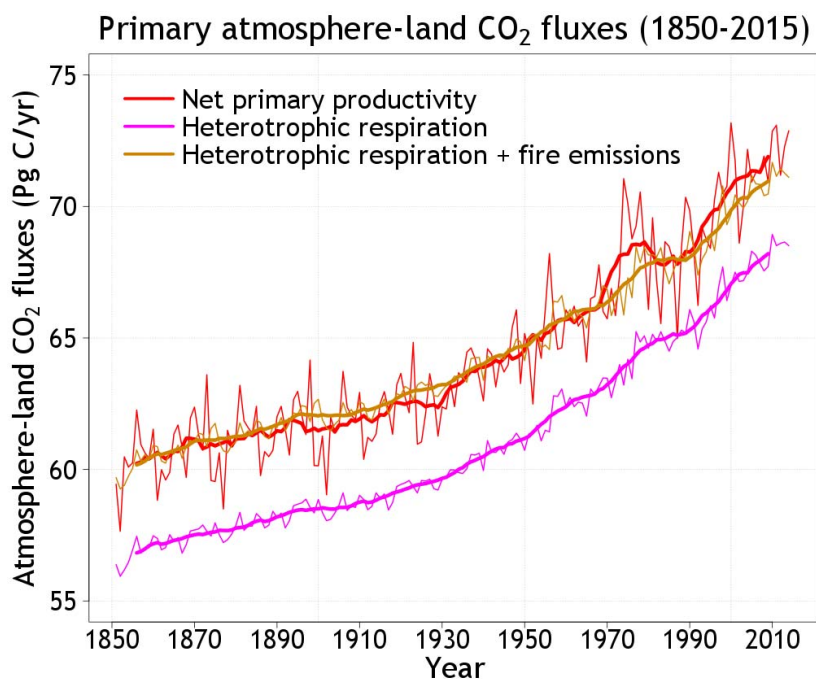
1435
1436
1437
1438
1439
1440

Figure 6: Time evolution of simulated natural methane fluxes (shown on the primary y-axis) and annual maximum wetland extent (shown on the secondary y-axis) by CLASS-CTEM for the 1851-2015 period in the transient historical simulation.



1441

1442



1443

1444

1445 Figure 7: Time evolution of simulated net primary productivity (NPP) and heterotrophic
1446 respiration in the historical simulation both of which increase in response to increase in
1447 atmospheric CO₂ concentration. The thin lines show annual values while the thick lines
1448 represent their 10-year moving average. When fire CO₂ emissions are added to heterotrophic
1449 respiration the total amount is equal to NPP especially during 1850s as the case should be
1450 when the system is in equilibrium and net atmosphere-land CO₂ flux (equal to NPP –
1451 heterotrophic respiration – fire emissions) is near zero. Later in the 20th century and early 21st
1452 century, NPP is greater than the sum of heterotrophic respiration and fire CO₂ emissions,
1453 which creates the sink over land that is currently observed.

1454

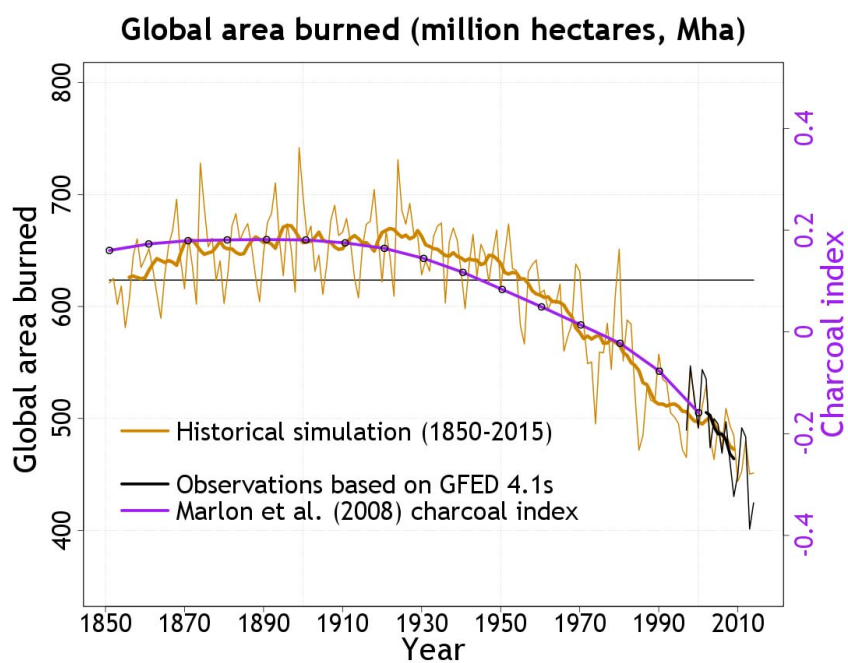
1455



1456

1457

1458



1459

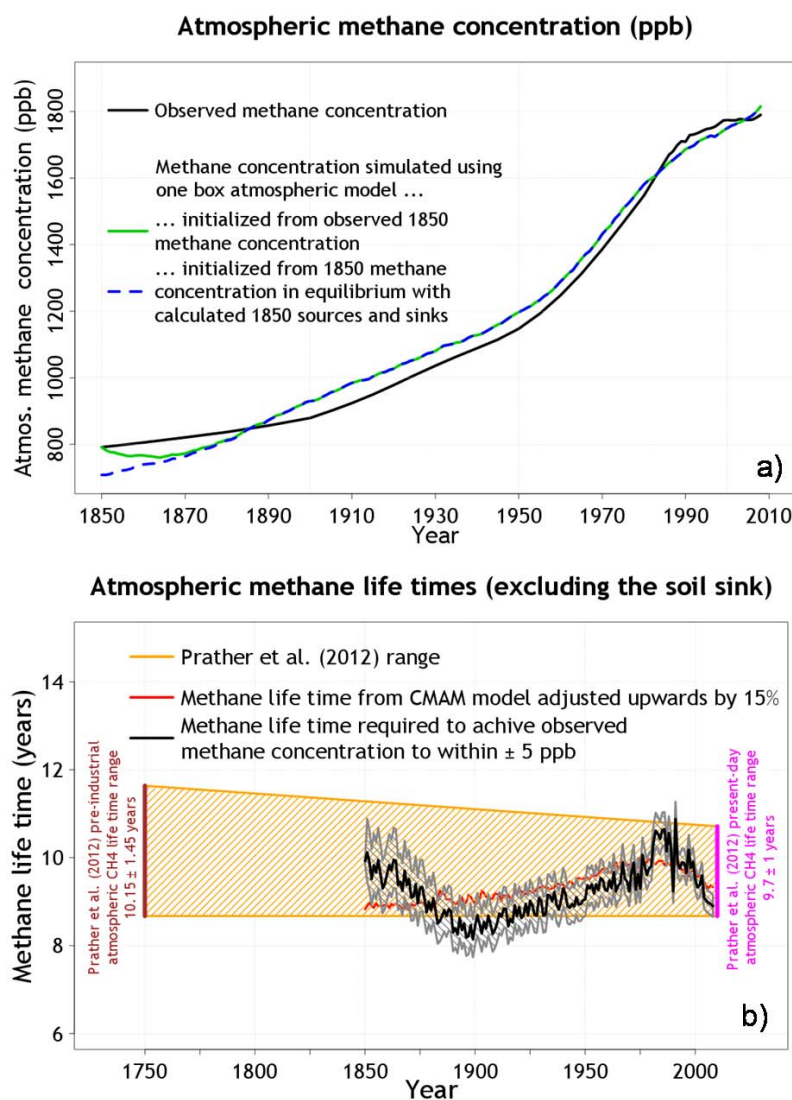
1460 Figure 8: Comparison of global area burned from the transient 1851-2015 historical
1461 simulation (dark yellow line). The thick dark yellow line is the 10-year moving average.
1462 Observation-based area burned (black line) are based on the GFED 4.1s data set. Model
1463 results are also compared to decadal charcoal index from version 3 of the Global Charcoal
1464 Database (purple line). Charcoal index is a proxy for burning and not for area burned per se
1465 and therefore only provides a qualitative measure.

1466

1467



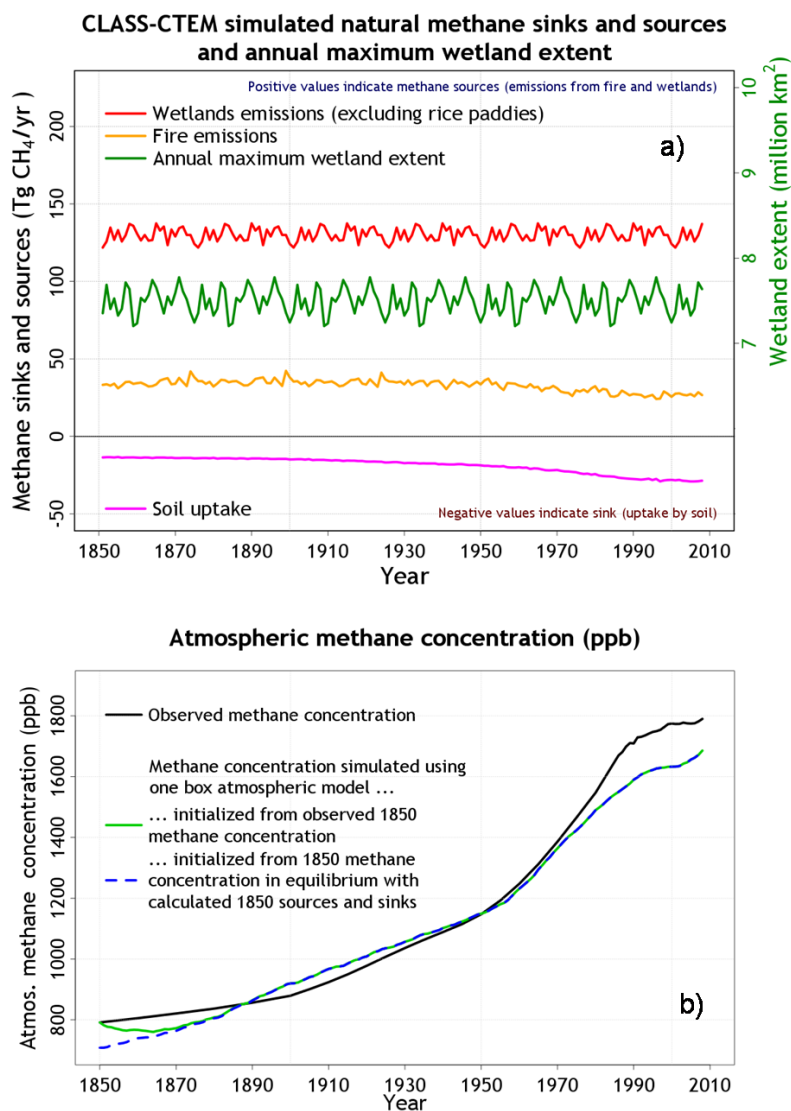
1468



1469 Figure 9: Comparison of simulated methane concentration over the historical period with its
 1470 observation-based estimates (panel a). The simulation may be initialized from the 1850
 1471 observed methane concentration (solid green line) or from an 1850 concentration that is in
 1472 equilibrium with 1850 specified methane sources and sinks (dashed blue line) as explained in
 1473 section 3.2. Panel (b) compares the methane lifetimes required to achieve the observed
 1474 increase in methane concentration over the historical period (black line) to within ± 5 ppb
 1475 (shaded area between grey lines) with observation-based estimate of atmospheric methane
 1476 lifetime based on Prather et al. (2012) and the adjusted atmospheric methane lifetime from
 1477 CMAM.
 1478



1479



1480

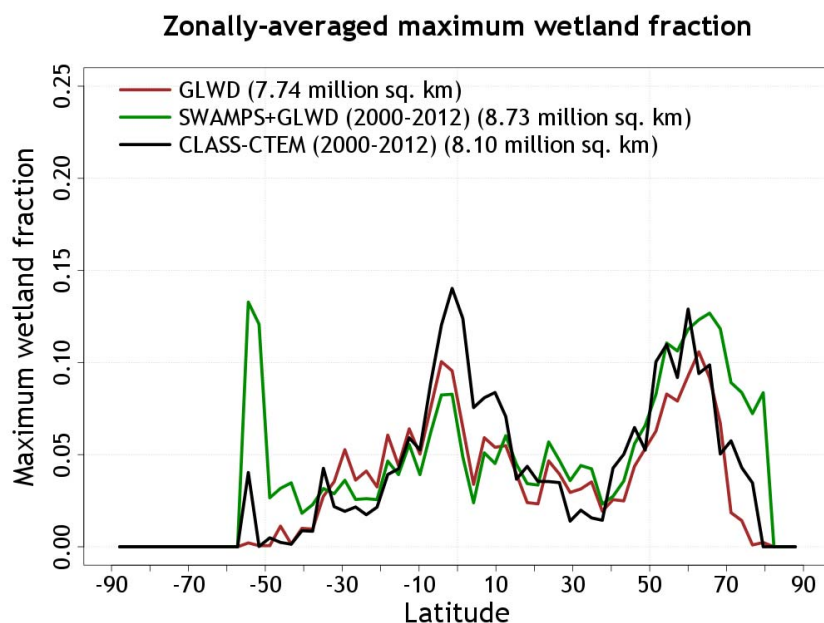
1481 Figure 10: Time evolution of simulated natural methane fluxes (shown on the primary y-axis)
1482 and annual maximum wetland extent (shown on the secondary y-axis) by CLASS-CTEM for
1483 the 1851-2008 period for the case when wetland extent and methane emissions are not
1484 allowed to respond to changing climate and increase atmospheric CO₂ over the historical
1485 period (panel a). Panel (b) shows the simulated methane concentration over the historical
1486 period, together with its observation-based values, when the natural fluxes shown in panel (a)
1487 are used within the framework of the one box model of atmospheric methane.

1488



1489

1490



1491

1492 Figure 11: Comparison of simulated zonally-averaged maximum wetland fraction over land
1493 with observation-based estimates based on the Global Lakes and Wetland (GLWD; Lehner
1494 and Döll, 2004) and a new product that is formed by merging remote sensing based
1495 observations of daily surface inundation from the Surface Water Microwave Product Series
1496 (SWAMPS; Schroeder et al., 2015) with the static inventory of wetland area from the GLWD
1497 as explained in Poulter et al. (2017).

1498

1499

1500

1501

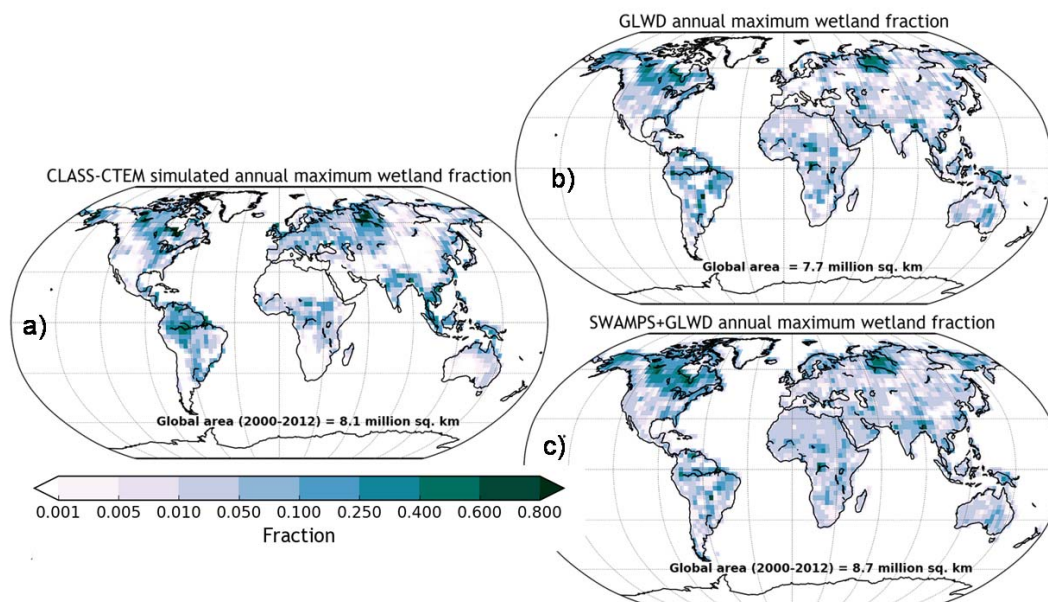
1502

1503

1504



1505
1506
1507

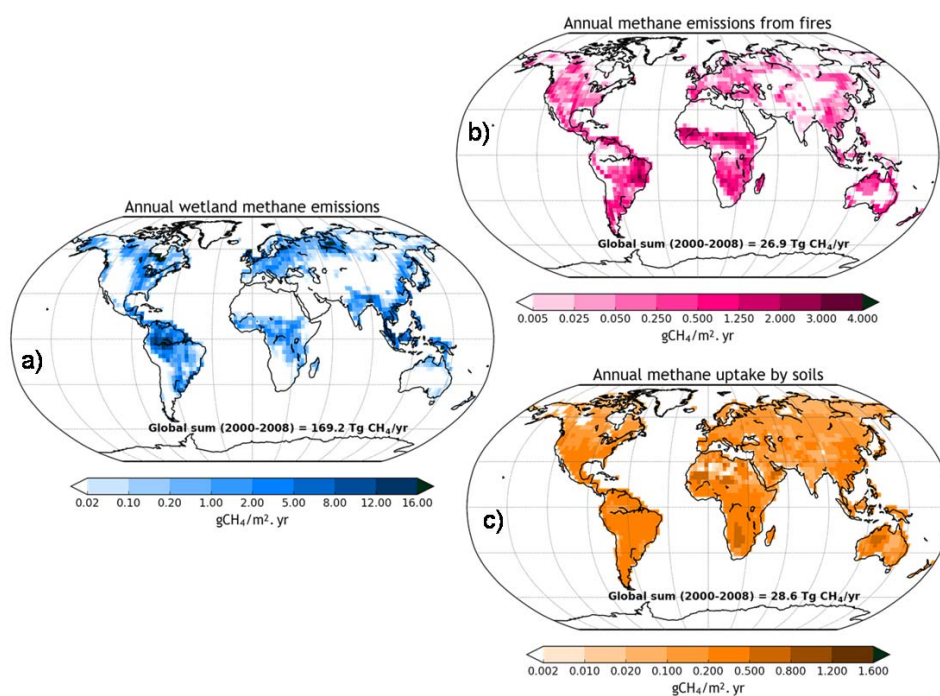


1508 Figure 12: Comparison of geographical distribution simulated annual maximum wetland
1509 fraction with observation-based estimates based on the Global Lakes and Wetland (GLWD;
1510 Lehner and Döll, 2004) and a new product that is formed by merging remote sensing based
1511 observations of daily surface inundation from the Surface Water Microwave Product Series
1512 (SWAMPS; Schroeder et al., 2015) with the static inventory of wetland area from the GLWD
1513 as explained in Poulter et al. (2017).

1514
1515
1516
1517
1518



1519
1520
1521
1522
1523
1524
1525

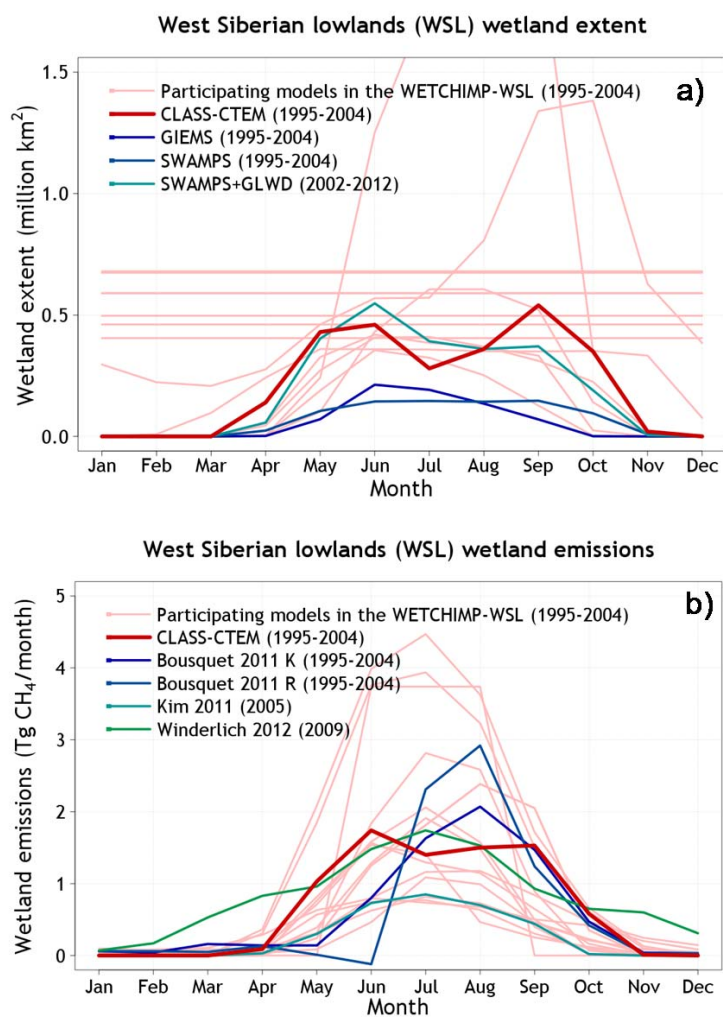


1526
1527
1528
1529
1530
1531

Figure 13: Geographical distribution of annual emissions from wetlands (panel a) and fire (panel c), and the soil sink (panel b) simulated by the CLASS-CTEM model. The data are averaged over the 2000-2009 period.



1532



1533

1534 Figure 14: Comparison of CLASS-CTEM simulated wetland extend (panel a) and wetland
1535 methane emissions (pane; b) over the West Siberian lowlands (WSL) region with those from
1536 models participating in the WETCHIMP-WSL intercomparison and observation- and
1537 inversion-based estimates as discussed in section 3.5.

1538

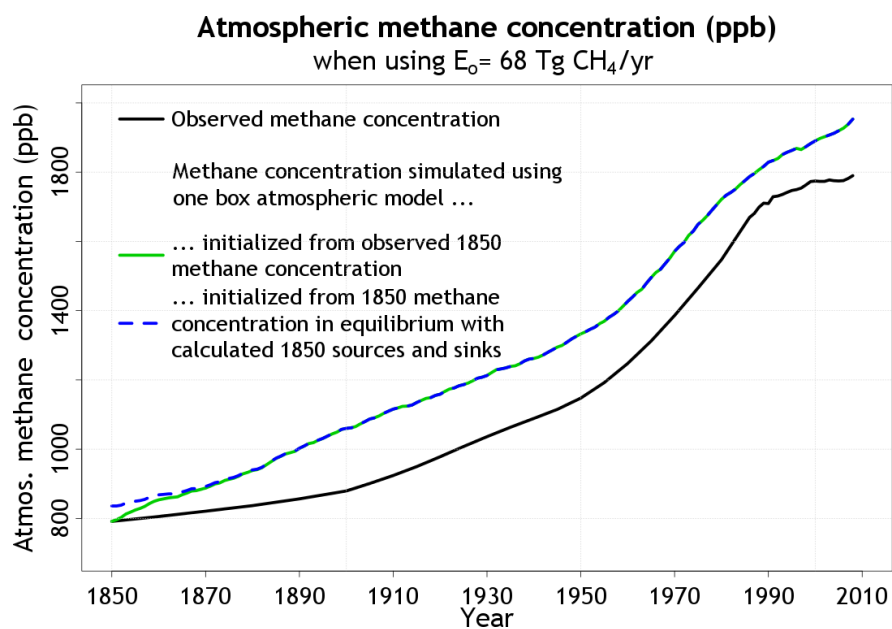
1539

1540

1541



1542
1543
1544



1545
1546
1547
1548
1549

Figure 15: Simulated methane concentration over the historical period, together with its observation-based values, when other non-wetland natural methane emissions (E_o) are specified at $68 \text{ Tg CH}_4/\text{yr}$ over the historical period.